View metadata, citation and similar papers at core.ac.uk

brought to you by CORE

provided by Syracuse University Research Facility and Collaborative Environment

Syracuse University

SURFACE

Theses - ALL

August 2018

Measuring Atmospheric Dry Deposition to Urban Surfaces

Alexander J. Johnson
Syracuse University

Follow this and additional works at: https://surface.syr.edu/thesis

 Part of the Engineering Commons

Recommended Citation

Johnson, Alexander J., "Measuring Atmospheric Dry Deposition to Urban Surfaces" (2018). *Theses - ALL*. 265.
https://surface.syr.edu/thesis/265

This is brought to you for free and open access by SURFACE. It has been accepted for inclusion in Theses - ALL by an authorized administrator of SURFACE. For more information, please contact surface@syr.edu.

Abstract

Surrogate surfaces are used to measure atmospheric dry deposition of contaminants, and are sometimes designed intentionally with simple geometry to estimate the lower limit of the flux to any surface. However, most surrogate surfaces have a small collection area: long periods of dry weather may be needed to obtain sufficient deposited contaminants to be detected and quantified, and such exposure periods may not be common in wet climates. In this study, two relatively large surrogate surfaces—disks with surface areas > 1 m^2—were designed to measure dry deposition of F^-, Cl^-, SO_4^{2-}, and NO_3^- in Syracuse, NY. Results indicate that good reproducibility is possible for measurements with exposure periods of 2-6 days. Computational Fluid Dynamics modeling shows that the boundary layer thickness varies somewhat over the disk, but average fluxes to different sections of the disk differ by only 8%. This study also proposes a new method to measure dry deposition to urban surfaces by measuring the removal of dry deposited material in runoff samples collected from an urban surface during a rainstorm at various time steps. For this method to work, the amount of dry deposited mass must be substantially greater than the amount contributed by precipitation. As an example calculation, the amount of SO_4^{2-} deposited to the roof of the War Memorial Arena in downtown Syracuse, NY is estimated using dry deposition data from the disks and compared to the amount of SO_4^{2-} in the precipitation for a hypothetical storm. The results show that it may be possible to measure the removal of SO_4^{2-} and other contaminants from the roof by stormwater runoff during a subsequent rainstorm.

MEASURING ATMOSPHERIC DRY DEPOSITION TO URBAN SURFACES

By

Alexander Johnson

B.S., Iowa State University, Ames, Iowa, 2014

Thesis

Submitted in partial fulfillment of the requirements for the degree of

Master of Science in Environmental Engineering.

Syracuse University

August 2018

Copyright © Alexander Johnson 2018

All Rights Reserved

Acknowledgements

I would like to express my sincere gratitude to my thesis advisor Dr. Cliff Davidson for his continuous support during my growth as a scientist, and for his patience, motivation, enthusiasm, and expertise. With his mentorship, I have matured not only as a scientist but also as an individual. I have gained a life-long professional connection through Cliff as I continue moving forward with my career.

I would like to acknowledge the support from the members of my committee: Dr. Charley Driscoll, Dr. Teng Zeng, and Dr. Eric Lui, who all provided constructive feedback on my research and challenged me with good questions. I would also like to thank the Center for Environmental Systems Engineering at SU, including manager Mario Montesdeoca, for use of laboratory instrumentation and facilities for my research. Additionally, I would like to thank academic coordinator Elizabeth Buchannan and department chair Andria Costello Staniec of Civil & Environmental Engineering for fostering a welcoming and pleasant environment and their continued support. Furthermore, I appreciate the support from the colleagues and friends I have gained throughout my journey at SU, including the MS and PhD students of the Cliff Davidson research group, several graduate students in the College of Engineering and EMPOWER program, and fellow members of the ASEE@SU executive board.

Last but certainly not least, I would like to thank my parents James and Cindy Johnson and my older sister Alison Johnson, who will always continue to support my endeavors no matter where I am in the world.

Table of Contents

Tables and Figures

List of Tables:

List of Figures:

Chapter 1: Introduction

Dry and wet deposition remove particles and gases from the ambient atmosphere, transferring them to natural surfaces such as soil and vegetation and human-made surfaces such as building roofs and pavement. Deposition is an important pathway for air contaminants to enter the environment (Mohan, 2016), and some contaminants have well-known impacts. Deposition of nitrogen (N as NO_2, NO_3^-, and HNO_3) can enrich the amount of nitrogen in soils and natural waters, depleting soil nutrients that contribute to soil fertility, acidifying surface waters, and reducing biodiversity in ecosystems (Vitousek et al., 1997). Deposition of sulfur (S as SO_2, SO_4^{2-}, and H_2SO_4) is also a significant contributor to acidification of ecosystems (Driscoll et al., 2018; Heard et al., 2014) and can affect the cycling and release of micronutrients and organic matter in soils (Monteith et al., 2007). Anthropogenic activities have increased atmospheric concentrations of trace metals, including lead (Pb), above prehistoric levels (Settle and Patterson, 1982), and these metals can deposit in terrestrial and marine ecosystems (Boyle et al., 2014; Chien et al., 2017; Fishwick et al., 2018). Mercury (Hg) emitted by industrial sources can also deposit in ecosystems (Lindberg et al., 2007) and poison wildlife (Wolfe et al., 1998). Atmospheric carbon, mainly particulate elemental and organic carbon, can deposit on buildings, forming black crusts (Bonazza et al., 2007; Hamilton and Mansfield, 1991). There is also interest in understanding dry deposition of polycyclic aromatic hydrocarbons (PAHs), which are emitted from biomass burning and oil and gas production (Zhang et al., 2015).

Wet deposition fluxes of contaminants can be measured by collecting precipitation samples. But measuring dry deposition is more complex, and it is often difficult to measure dry deposition directly to natural and human-made surfaces. Therefore, the flux of a contaminant is obtained by calculating the product of the atmospheric airborne concentration (measured at some height

above the surface) and the dry deposition velocity. The deposition velocity (usually expressed in cm s^{-1}) is estimated with mathematical functions based on particle size (Nicholson, 1988). Other factors that influence the deposition velocity include surface characteristics (canopy structure, stomatal conductance, pH, etc.), local meteorology (surface roughness, wind speed, temperature, etc.), and the properties of the depositing material (density, solubility, shape, etc.). These variables are further discussed in Sehmel (1980). Given the number of factors that can affect the deposition velocity, modeled estimates are highly parameterized. Therefore, while atmospheric concentrations of a contaminant at two sites may be similar, the deposition velocities can be different (Schwede et al., 2011). Time-averaged fluxes computed using modeled dry deposition velocities can also result in large uncertainties (Ban et al., 2016; Endo et al., 2011; Erisman et al., 1994). Inferring deposition of contaminants using modeled dry deposition velocities on a regional scale is also associated with uncertainties due to sparse data coverage, biases at locations far from the original emission sources (Liu et al., 2017), and errors from interpolating dry deposition with varying land cover and surface characteristics (Im et al., 2013). Regional dry deposition models can have uncertainties of 50% (Fowler et al., 2009). With these uncertainties, measured deposition velocities could be useful for comparison with modeled estimates and for obtaining a range of possible values to a complex surface.

Dry deposition velocities can be measured by the use of surrogate surfaces. The accumulated material on the surrogate surface is extracted and analyzed for the chemical species of interest, and therefore surrogate surfaces allow for direct estimates of the dry deposition flux (Holsen and Noll, 1992). By simultaneously measuring the flux of a contaminant using the surrogate surface and its airborne concentration, the dry deposition velocity for that contaminant can be computed by dividing the flux by the airborne concentration.

Surrogate surfaces used in early studies include petri dishes, Teflon plates and filters, and dustfall buckets (Dasch, 1985; Davidson et al., 1985). More recent surrogate surface designs include the symmetric airfoil and the knife-edge surrogate surface (McCready, 1986; Wu et al., 1992a) these surfaces are designed to collect less deposition than natural and human-made surfaces (Mohan, 2016), enabling an estimate of the minimum flux to the complex surface of interest. The deposition plate in the center of the symmetric airfoil has also been modified with a water surface to collect gases such as SO_2 (Yi et al., 1997) as well as with artificial turf to better mimic the roughness elements of a natural surface (Hall et al., 2017; Lynam et al., 2015). Therefore, deposition velocities obtained using the symmetric airfoil and the knife-edge surrogate surface are lower limits to a range of values for a complex surface, with modeled estimates as a possible upper limits.

Numerous studies have used surrogate surfaces to compute dry deposition velocities of particulate chemical species. Some studies with simultaneous measurements of SO_4^{2-} and NO_3^- include Wu et al. (1992a), Saxena et al. (1992), Chen et al. (1996), and Lestari et al. (2003). While small particles of SO_4^{2-} and NO_3^- dominate airborne concentrations, large particles are often responsible for most of the dry deposited mass to surrogate surfaces (Davidson et al., 1985). Studies that have measured a wide variety of trace metals include Zufall and Davidson (1998), Yun et al. (2002), Wai et al. (2010) and Chu et al. (2008). Huang et al. (2014) compiled a review of dry deposition measurements of Hg. Metals derived from soil and mineral dust, such as Ca, usually have larger deposition velocities than metals derived from anthropogenic emissions, such as Pb (Yi et al., 1997). Deposition of elemental and organic carbon is usually not measured with surrogate surfaces, but organic chemical species such as PAHs have been measured with surrogate surfaces by Sheu et al. (1996), Chang et al. (2003), Tasdemir et al.

(2007), Bozlaker et al. (2008), and Eng et al. (2013); these studies showed that deposition velocities of PAHs with low volatilities were greater than deposition velocities of PAHs with high volatilities.

In this study, four symmetric airfoils were deployed for dry deposition experiments in 2015 and 2016 to measure fluxes and dry deposition velocities of inorganic anions and trace metals at a single site in Syracuse, NY. Experiments were conducted at Syracuse University on the roof of the Biological Research Laboratories (BRL), and exposure of the airfoils was usually 2-4 days. However, the results from each experiment showed that the amount of dry deposited masses in the samples were nearly indistinguishable from the masses in the blanks for chemical species such as Pb and F, which have low atmospheric concentrations. There was also poor agreement among the samples for all chemical species, suggesting that the data were not reproducible. Because of the small collection area of the symmetric airfoils, the amount of dry deposited mass collected was 10-30 μg for many chemical species. Because of the small amount of dry deposited masses, the samples were highly sensitive to contamination from sample handling, and slight inconsistencies during extraction of samples led to significant errors. To increase the amount of dry deposited masses, two options were proposed: increase the number of dry days for each experiment or increase the collection area. The former option was not necessarily feasible, and therefore two large disks were designed and built to increase the amount of dry deposition mass collected during each experiment.

Dry deposition data obtained from surrogate surfaces can also be used to quantify the dry deposition of contaminants to building roofs. The disks can potentially mimic some of the characteristics of a flat building roof, namely both are smooth, flat horizontal surfaces, although some building roofs may have HVAC systems, pipes, and other obstructions that could increase

deposition. Therefore, dry deposition fluxes measured using the disks may be a minimum of the flux to a building roof. Multiplying the flux from the surrogate surface by the surface area of the roof and the antecedent dry period (ADP) yields the mass of contaminant deposited to the roof.

Dry deposited contaminants on a roof can be removed during a subsequent rainstorm. The removal of dry deposition can potentially be measured in the runoff if the amount of contaminant in the runoff contributed by dry deposition is substantially greater than the amount in the precipitation as well as the error in the measurement. During the beginning of the rainstorm, concentrations of that contaminant in the runoff will decrease to the same level as the concentration in the precipitation, indicating removal of dry deposited material.

The objectives of this study are to determine if the two disks can be used to obtain consistent dry deposition data of inorganic anions in Syracuse, NY, and whether deposition is uniform on the disks. Because not much is known on deposition to large surrogate surfaces, the data presented in this study are compared to data from studies that estimated deposition using smaller surfaces. The results of these experiments are presented in Chapter 2.

Future work is discussed in Chapter 3. The objective of this future work is to determine if it is possible to measure the removal of dry deposited SO_4^{2-} from a roof during a rainstorm. The roof for these experiments will be on the War Memorial Arena in downtown Syracuse, NY.

Chapter 2: Measuring dry deposition using large surrogate surfaces for improved time resolution

2.1 Introduction

Aerosols and gases can degrade urban surfaces exposed to the atmosphere. For example, SO_4^{2-} and NO_3^- can damage marble, bronze, and other materials used in historic monuments (Livingston, 2016). Airborne Cl^- from sea salt can erode concrete infrastructure in coastal regions (Anwar Hossain et al., 2009; Meira et al., 2007). Elemental carbon aerosol can soil both vertical and horizontal surfaces of buildings (Etyemezian et al., 1998). But to quantify the amount of damage to these surfaces, we need to estimate the dry deposition fluxes of contaminants to these surfaces.

While it is difficult to measure or model aerosol dry deposition to urban surfaces of varying geometry and surface roughness, measurements using a smooth surrogate surface of simple geometry can provide estimates of the minimum flux onto any surface under similar atmospheric conditions. Some examples of surrogate surfaces include the symmetric airfoil (Wu et al., 1992a), the knife-edge surrogate surface (McCready, 1986), and the water collector (Yi et al., 1997). These surfaces have been used to measure dry deposition fluxes of inorganic anions such as Cl^-, SO_4^{2-}, and NO_3^- (Chu et al., 2008; Lestari et al., 2003; Tasdemir and Günez, 2006; Wu et al., 1992b) and also trace metals (Tasdemir and Kural, 2005; Zufall et al., 1998) and organic compounds (Holsen et al., 1991; Tasdemir et al., 2004).

Surrogate surfaces collect mainly coarse particles (> 2.5 μm) that efficiently pass through the quasi-laminar boundary layer by settling, turbulent inertial deposition, or impaction (Friedlander, 1977; Seinfeld and Pandis, 2016). Dry deposition velocities of coarse particles—defined as the

coarse particle flux (g m^{-2} day^{-1}) divided by the coarse particle airborne concentration (g m^{-3})—are usually > 0.1 cm/s, depending on particle, surface, and atmospheric characteristics (Giardina and Buffa, 2018; Sehmel, 1973). In contrast, dry deposition velocities of submicron particles in the 0.1-1 μm range are usually < 0.1 cm/s (Horvath et al., 1996; Roupsard et al., 2013); these particles do not efficiently diffuse through the boundary layer. At most locations, the bulk of the airborne particle mass is generally in the 0.1-1 μm range (Seinfeld and Pandis, 2016), but most of the particle mass deposited onto a surrogate surface is coarse (Wu et al., 1992a). The dry deposition velocity computed as total flux / total airborne concentration must therefore be interpreted carefully since measured values of the flux and airborne concentration result from different size ranges. Dry deposition velocities reported in the literature are usually calculated as the total flux / total airborne concentration.

Another problem is that many surrogate surfaces have a small collection area that may require long exposure periods to obtain signals above the detection limits and blank levels, particularly for contaminants with low atmospheric concentrations. For example, the mean atmospheric concentration of F^- in the U.S. is usually no more than 0.1 μg m^{-3} (Liteplo et al., 2002). Controls and regulations on emissions have also caused lower concentrations of atmospheric particulate SO_4^{2-} and other chemical species in the U.S. (Chan et al., 2018; Hand et al., 2012). But long exposures may not be possible in regions with frequent rain and snow. Thus, a surrogate surface with a larger surface area (> 1 m^2) could offer opportunities to sample for short exposures and for chemical species found at low concentrations.

In this study, I present dry deposition measurements of particulate F^-, Cl^-, SO_4^{2-}, and NO_3^- using large surrogate surfaces—disks of just over 1 m^2—exposed on a building roof. The goals were (1) to determine whether consistent anion dry deposition data could be obtained with the disks

over short exposures at typical airborne concentrations in Syracuse, NY, and (2) to examine deposition as a function of position on the disk by measuring the flux on four sections of the disk, and by modeling the ambient wind speed over the disk using computational fluid dynamics (CFD) to examine if the quasi-laminar boundary layer varies significantly in thickness.

2.2 Materials and Methods

2.2.1 Description of field site and sampling equipment

Experiments were conducted on the roof of the Biological Research Laboratories (BRL) at Syracuse University (SU) in Syracuse, NY. BRL is ~ 30 m high and overlooks the campus quad to the west and several shorter buildings to the east and west. A steep hill rises to the south. Figure 2.1 is a diagram of the roof with the locations of the sampling equipment and the roof dimensions. The penthouse occupies most of the north edge of the roof and is ~ 3 m in height. Two or more parallel Teflon PTFE filters (polytetrafluorethylene, Item Number: 722PTPT, Zefon International Inc., Ocala, FL) were connected to a vacuum pump—each filter with its own rotameter (Model Number: FL2015, Omega Engineering, Stamford, CT). The rotameters were calibrated with a Gilibrator (Sensidyne, Clearwater, FL).

BRL is ~ 180 m from a weather station on the roof of the Center for Science and Technology building on campus. The weather station was installed in 2017 and records data every minute. Data on wind direction were downloaded for experiments conducted in 2017 and 2018. The mean wind direction ranged from 130-240° (SE-WSW) for these experiments.

The two surrogate surfaces deployed in the field are shown in Figure 2.2. Each disk is 1.2 m (48 inches) in diameter and 0.32 cm (1/8 inch) thick. The disk is polyethylene, and smooth Teflon FEP film (fluorinated ethylene propylene, Bytec® Corporation) is wrapped around the disk to

serve as the deposition surface and to protect the disk against sunlight and harsh reagents. A drain hole with a diameter of 2.54 cm is at the center of the disk; a bottle is placed under the drain while collecting samples. The total height of each assembly is ~ 1.2 m.

2.2.2 Experimental Procedures: Dry deposition and airborne concentration measurements

Several experiments were conducted to measure dry deposition fluxes onto the disks and simultaneous airborne concentrations. The date, total exposure period, number of samples and blanks prepared from the disks, and number of air filters deployed for each experiment are shown in Table 2.1. An experiment consisted of (i) preparing blanks, (ii) exposing the disks, and (iii) collecting samples. The exposure period was defined as the time from the end of the collection the last field blank to the collection of the first deposition sample.

Prior to each experiment, glass sample bottles, Teflon PFA vials (perfluoroalkoxy alkane), and Teflon PTFE forceps and scrapers were cleaned with methanol and Milli-Q® water (18.2 MΩ cm resistivity). These items were dried overnight. Scrapers were double-bagged in sealed clean bags. High-density polyethylene spray bottles were filled with Milli-Q® water and transported from the lab to BRL in Ziploc bags.

At the beginning of each experiment, air filters were run for 1 minute as blanks, and then sample filters were deployed—all without denuders. Sampling was not isokinetic. The flow rate through the rotameters was usually recorded at least twice per day during each experiment. At the end of the experiment, filters were re-capped and stored in their casings in a clean room (usually for < 1 week). The filters were submerged in 10-11 mL of Milli-Q® water inside PFA vials and extracted with ultrasound at a frequency of 37 kHz for 30 minutes. The extracts were poured into separate vials and stored at 5°C. For some experiments, the sample filters were extracted a second time to verify that the first extraction removed all material from the filter.

Prior to exposure, the disks were wiped with low-lint cloths soaked with high-purity methylene chloride, sprayed with Milli-Q® water, and then wiped dry. Blanks were then prepared from each disk: Milli-Q® water was sprayed onto the surface of the disk and scraped into the bottle underneath the drain hole a total of three times for each blank. This procedure was repeated two more times, yielding three blanks for each disk (from the nine scrapings of that disk). After the procedure, the scrapers were cleaned and bagged again until sample collection.

Samples were collected after exposure using the same procedure: Milli-Q® water was sprayed onto the disk, and the water and particles on the disks were scraped into a bottle underneath the drain hole. The procedure was usually repeated two more times, providing three consecutive samples that could be compared to determine if all of the deposited material was removed from the disk. Blanks and samples collected from the disks were weighed and stored at 5°C until analysis.

Two experiments were conducted to determine how fluxes differ on the four sections of the disk (indicated by asterisk in Table 2.1). The surface areas of sections one, two, three, and four were 0.58, 0.24, 0.22, and 0.11 m^2, respectively. Section four was assumed as the leading edge based on wind direction data. Strips of FEP film were used to mark the sections. Blanks were collected from section one. To examine wind direction for both experiments, hourly data were downloaded from the Syracuse Hancock International Airport, which is 8 km north of campus (http://www.ncdc.noaa.gov).

2.2.3 Chemical and data analysis

Samples and blanks were usually analyzed within 2 weeks after collection. Analysis of F, Cl^-, SO_4^{2-}, and NO_3^- was conducted by ion chromatography (DX 500, Dionex™, Sunnyvale, CA). All analytical runs were calibrated with 4-6 standards (IC Check Standard #1, SPEX CertiPrep®,

Metuchen, NJ). A calibration standard and laboratory blank were analyzed after each batch of 10 samples. The recovery of the calibration standard was 90-110%. Only calibration curves with an $R^2 \geq 99.5\%$ were accepted.

Ten laboratory blanks were analyzed to compute the limit of detection (LOD) and limit of quantification (LOQ) for each analytical run. The LOD was defined as the average of the 10 laboratory blanks plus 3 times the standard deviation; the LOQ was taken as ten times the LOD. Concentrations below the LOD were replaced with zero, and concentrations between the LOD and LOQ were flagged but still used for analysis—filter blanks were sometimes in this range. All other sample and blank concentrations were above the LOQ.

The mass of each anion was computed for all samples. The net mass deposited to each disk was calculated as the sum of masses in the three consecutive samples on a disk, minus the average blank for that experiment. The average blank for an experiment was computed by summing the masses of the three consecutive blanks on each disk, and then taking the average of the two sums. Thus, it was assumed that each sample contained a level of contamination equal to the average blank. For the two experiments investigating the differences in the flux across sections of the disk, the mass deposited to each section was calculated, and the masses for all four sections were summed to estimate the total mass deposited. Blank values were computed for each section by scaling the mass from each blank by the area of that section; these calculations assumed that contamination was distributed evenly across the disks.

The dry deposition flux onto each disk was calculated in $\mu g\ m^{-2}\ day^{-1}$, and the values from the two disks were averaged. Filter samples were blank corrected and then averaged to obtain the average particulate airborne concentration in $\mu g\ m^{-3}$ for each anion. Only average masses that

were 5 times greater than the average of the blanks were accepted to compute dry deposition fluxes and airborne concentrations.

The average dry deposition velocity was computed in cm/s for each anion. Standard deviations of the dry deposition velocities were computed by compounding the standard deviations of the dry deposition fluxes and airborne concentrations (formula is shown in Appendix).

2.2.4 CFD modeling

ANSYS Fluent was used to solve the 2-D (x, y) velocity field. An inlet wind speed of 3 m/s was chosen based on the average wind speed recorded on the Center for Science and Technology for the Feb. 17-21, 2017 experiment. The local Reynolds number, based on distance across the disk, is unlikely to exceed 500,000 where the boundary layer becomes turbulent (Schlichting and Gersten, 2000). But on a rooftop, there could be sufficient atmospheric turbulence to cause a transition from a laminar to a turbulent boundary layer. To capture any transition effects on boundary layer structure, the Transition (γ-Re_θ) Shear Stress Transport model was selected. This model can also sufficiently capture boundary layer separation and reattachment under low-Re flows (Aftab et al., 2016). An inlet turbulence intensity of 25% was chosen as a possible value for BRL based on measurements of the turbulence intensity on a roof ~ 11 m tall; values typically ranged from 20-60% (Carpman, 2011). All FLUENT runs assumed an air density and viscosity with T = 20°C. Residuals converged to less than 10^{-9}.

The model was rerun with successively finer grids until grid independence was achieved, and the number of grids near the surface of the disk was also increased until $u^*y/\upsilon < 5$ (dimensionless) to resolve the viscous sublayer, where u^* = friction velocity (cm/s) of the air, y = distance to the surface (cm), and υ = kinematic viscosity of the air (cm^2/s). For the final model, $u^*y/\upsilon \leq 0.2$.

The model was also rerun with different turbulence intensities; changes in turbulent properties were observed but changes in the boundary layer structure were negligible.

In ANSYS CFD-Post, vertical lines were plotted at five positions on the disk; these positions are designated as A, B, C, D, and E, and are shown in Figure 2.3. For each line, the velocity in the x-direction was computed from the surface of the disk to 1.5 cm above it.

2.3 Results and Discussion

Results show that good reproducibility is possible with the disks. The dry deposition flux between the two disks varies on average for all experiments by 7.2%, 9.3%, 8.5%, and 6.7% for F^-, Cl^-, SO_4^{2-}, and NO_3^-, respectively (Wilcoxon rank-sum test; $p >> 0.05$).

The fluxes reported in this study are conservative estimates because the three consecutive blanks are summed for each disk, which probably overestimates the blanks. The third blank is usually the smallest of the three values. Since the mass usually decreases with subsequent scrapings, it is likely that the masses in the first two consecutive blanks are greater than the contamination in the sample, which is mainly a result of contaminants introduced during sample handling such as dust and sweat. If only the mass in the third and final blank is considered, the average flux is larger, and the standard deviation is smaller. Therefore, the percent differences in the fluxes between the two disks, if only the third blank is used, are smaller than the values reported above.

Even with the overestimated blank values, the ratios of the average mass in the sample to the average mass in the blank are nearly all > 10 for each anion. The average ratios for all flux data are 14, 35, 39, and 18 for F^-, Cl^-, SO_4^{2-} and NO_3^-, respectively. While ratios are generally lower for F^- and NO_3^-, most values < 5 are for Cl^-; methylene chloride efficiently removed dirt on the surface of the disks but probably increased Cl^- levels in the blanks for these experiments.

Although grease is sometimes used in dry deposition experiments to minimize resuspension, it was not applied to the disks. This is because the high background levels of each anion in the grease and the handling from applying and removing the grease could contaminate both the blanks and the samples. Thus, the dry deposition data reported here include the effects of both deposition and resuspension.

Of the three consecutive samples, the first sample on average accounts for 90-99% of the total dry deposited mass of each anion after correcting for blank levels. The dry deposited mass in the third consecutive sample from each disk is nearly indistinguishable from the average mass of the blanks (Wilcoxon-signed rank test; $p > 0.05$). Therefore, nearly all dry deposited mass is most likely removed from the disks in the first two consecutive samples.

The disks and air filters have been used to obtain dry deposition velocities of each anion for exposure periods ≤ 6 days (Table 2.2). Dry deposition velocities of Cl^-, SO_4^{2-}, and NO_3^- are generally within ranges of previously published values, which include measurements to both smooth and complex surfaces (MacLeod et al., 2011).

Dry deposition velocities of Cl^- are in the range 1.9-2.4 cm/s during the summer and fall and in the range 5.5-9.2 cm/s during the winter. Values from this study are generally higher than those measured using ungreased symmetric airfoils over Lake Erie (Zufall et al., 1998) and the values in Hong Kong measured using ungreased petri dishes (Tanner et al., 2001); the dry deposition velocities from these studies range 1 to 2 cm/s. Summer and fall dry deposition velocities from this study are lower than the average value of 4.1 cm/s measured using ungreased knife-edge surrogate surfaces for Taiwan (Chu et al., 2008) while winter values are higher.

Seasonal differences in the fluxes and airborne concentrations of Cl^- are apparent. The fluxes are > 1000 μg Cl^- m^{-2} day^{-1} during the winter compared to the average flux of 50 μg Cl^- m^{-2} day^{-1} during the summer and fall. Airborne concentrations (Table 2.3) vary from 0.15 to 1.5 μg Cl^- m^{-3} during the winter compared to the average of 0.03 μg Cl^- m^{-3} during the summer and fall. Because the airborne concentrations do not increase as much as the fluxes, the deposition velocities are higher in the winter by a factor of about 3. This pattern is consistent with the concept that the increase in flux is due to the largest airborne particles, but these particles have a slightly smaller influence on the total airborne concentration since submicron particles dominate the airborne concentration. It is likely that the increase in the Cl^- airborne concentration and flux is due to resuspension of deicing salt applied to the sidewalks and streets (Kolesar et al., 2018; Kumar et al., 2012). However, evaporation of Cl^- from the Teflon filters in summer may have contributed to the low airborne concentration data as well.

Dry deposition velocities of SO_4^{2-} range from 1.1 to 1.8 cm/s during the winter—nearly an order of magnitude higher compared to the range 0.11 to 0.39 cm/s in the summer and fall. Despite seasonal differences, these values are comparable to studies reported using other surrogate surfaces. The average SO_4^{2-} deposition velocity for the summer and fall in this study is 0.19 cm/s, which is just slightly less than average of 0.23 cm/s with greased symmetric airfoils for Gettysburg, PA (Wu et al., 1992a), and the values of 0.25 and 0.23 cm/s using ungreased petri dishes (Tanner et al., 2001). The deposition velocities of SO_4^{2-} measured using greased knife-edge surrogate surfaces at various locations for southern Taiwan range from 0.14 to 1.2 cm/s (Chen et al., 1996). However, average values measured using greased knife-edge surrogate surfaces are 3.0 and 7.5 cm/s at separate locations in Turkey (Tasdemir and Günez, 2006). Both

the airborne concentrations and fluxes are nearly two orders of magnitude greater than those in this study. These authors report unusual conditions due to excessive coal and oil consumption.

Deicing salt can contain up to 4% $CaSO_4$ as an impurity (Pitt et al., 1987). Therefore, deposition of deicing salt may also have enhanced the dry deposition flux of SO_4^{2-} during the winter: fluxes are 5-8 times larger compared to the summer and fall despite no apparent increases in the airborne concentration, reinforcing the idea that the increase in deposition of the largest SO_4^{2-} particles has a somewhat smaller influence on the total airborne SO_4^{2-}, which is mainly submicron.

Dry deposition velocities of NO_3^- range from 0.1 to 1.1 cm/s. This range is comparable to the range 0.1-1.2 cm/s measured using greased knife-edge surrogate surfaces (Chen et al., 1996) as well as the average of 0.6 cm/s measured using ungreased symmetric airfoils in southern California (Wu et al., 1992a). Values from this study are generally higher than values of 0.35 and 0.29 cm/s measured using ungreased petri dishes (Tanner et al., 2001) and the average of 0.27 cm/s measured using an ungreased knife-edge surrogate surface (Chu et al., 2008). The airborne concentrations of NO_3^- reported by Tanner et al. (2001) did not include denuders while those measured by Chu et al. (2008) included denuders.

Fluxes of NO_3^- do not differ by season, with values ranging from 110 to 380 μg NO_3^- m^{-2} day^{-1}. But airborne concentrations of NO_3^- in winter exceed those in summer and fall on average by nearly a factor of 2, which may explain some of the smaller dry deposition velocities in winter. More atmospheric submicron NH_4NO_3 may exist in colder temperatures since the dissociation constant decreases with temperature (Stelson and Seinfeld, 1982). Greater partitioning of NO_3^- to the aerosol phase in colder weather and/or lower volatility of the aerosol NO_3^- collected by the air filters could also explain increases in the airborne concentration. However, a significant

fraction of particulate aerosol NO_3^- deposited to the disks may have originated from heterogeneous reactions of NO_x with Ca^{2+} containing aerosol—an irreversible process producing NO_3^--containing coarse particles (Mamane and Gottlieb, 1992; Usher et al., 2003; Wolff, 1984). Due to the proximity of Interstate 81 (~ 0.8 km away) and other well-traveled roads, there is a continual input of NO_x at BRL from vehicle exhaust that can react with road and soil dust.

Dry deposition velocities of F^- range from 0.6 to 2.5 cm/s, with slightly lower values during the winter because of slightly higher airborne concentrations. While dry deposition of F^- is not well studied, calculated yearly average dry deposition velocities range from 1.2 to 2.5 cm/s in the Netherlands using the resistance model (Slooff et al., 1990); several of the values in Table 2.2 are within this range.

Fluxes range from 0.45 to 4.3 μg F^- m^{-2} day^{-1} and do not vary with season. Sources of airborne F^- include coal combustion and industrial activities such as manufacturing of metals (aluminum, copper, and nickel), steel, ceramics, glass, phosphate fertilizers, and adhesives (Lewandowska et al., 2013). These industries do not have a major presence in Syracuse, which may explain airborne concentrations of 1-4 ng F^- m^{-3}. But some industrial sources are found in cities to the west—the predominant upwind direction. Gaseous F^- may participate in heterogeneous reactions with soil and road dust containing SiO_2, contributing to the aerosol fraction (Slooff et al., 1990).

Weekly airborne concentration data of particulate Cl^-, SO_4^{2-}, and NO_3^- for five rural locations in Upstate New York from CASTNET https://www.epa.gov/castnet were downloaded for comparison with airborne concentration data from this study for 2016-2018. The average airborne concentration of Cl^- across the five sites was 0.04 +/- 0.05 μg Cl^- m^{-3}. Values were not necessarily larger during the winter, suggesting that the airborne concentrations may be less influenced by deicing salt in rural locations compared to urban locations such as Syracuse, where

airborne concentrations from this study and those measured in many cities in the Northeast U.S. (Kolesar et al., 2018) showed large increases during the winter. The average airborne concentrations of SO_4^{2-} and NO_3^- measured at CASTNET sites were 0.76+/- 0.3 µg SO_4^{2-} m^{-3} and 0.41 +/-0.46 µg NO_3^- m^{-3}. Airborne concentrations of SO_4^{2-} and NO_3^- from this study are also generally < 1 µg m^{-3}, suggesting that measurements in Syracuse are comparable to those measured at rural locations for these anions. No airborne concentrations of F^- are available from CASTNET, but the values reported in this study are less than 0.1 µg F^- m^{-3}, which is expected at locations away from industrial sources (Liteplo et al., 2012).

Because dry deposition velocities of anions are > 0.1 cm/s, coarse particles most likely account for a significant fraction of the dry deposition flux. These dry deposition velocities are calculated as the total flux/total airborne concentration. Dry deposition velocities based only on coarse particles would be much greater for all of these anions.

Previous studies in urban areas found that coarse particles account for most of the dry deposition fluxes of SO_4^{2-} and NO_3^- to the knife-edge surrogate surface (Lestari et al., 2003; Yang et al., 2005, 2004). In fact, Yang et al. (2005) report deposition velocities of NO_3^- that are comparable to sedimentation velocities, with values > 1 cm/s. While deposition velocities of NO_3^- are generally lower in this study, Yang et al. (2005) controlled for resuspension; no deposition velocities are reported in Lestari et al. (2003) and Yang et al. (2004) for comparison of SO_4^{2-}, but the fluxes measured in those studies are at least three orders of magnitude greater. Because BRL is located in a heavily trafficked area, vehicles most likely resuspend coarse particles (Patra et al., 2008), which may account for a significant fraction of the dry deposition flux.

On the other hand, dry deposition velocities of Cl^- and NO_3^- may have been overestimated because NO_3^- and Cl^- may have evaporated from the Teflon air filters during sampling,

depending on the temperature and relative humidity of the atmosphere (Liu et al., 2015). The ratio of the gas phase concentration to the particle phase concentration of NO_3^- may also be important (Zhang and McMurry, 1992). Evaporation of NO_3^- and Cl^- may be severe: Liu et al. (2014) reported that 49-89% of the NO_3^- and 60-88% of the Cl^- collected on Teflon filters evaporated during sampling, and additional NO_3^- and Cl^- evaporated from the filters during storage. Since deunders were not used in this study, the evaporated mass from the air filters cannot be quantified.

The correlation between the dry deposition flux and the airborne concentration was low for SO_4^{2-} and NO_3^- ($R^2 < 0.01$), consistent with the idea that submicron aerosols do not have a major influence on the dry deposition flux. In addition, no attempts were made to conduct isokinetic sampling, suggesting that many of the largest airborne particles were collected by the filters with low efficiency. The correlation between the dry deposition flux and the airborne concentration was stronger for F^- ($R^2 = 0.37$) and Cl^- ($R^2 = 0.965$). The high correlation for Cl^- should not be interpreted to suggest that the particles dominating the airborne concentration are the same as those depositing on the disks. Rather, the correlation may reflect two regimes based on season: low airborne concentrations and fluxes in the summer and fall are in contrast with slightly higher airborne concentrations and much higher fluxes in the winter. Two widely separated clusters of points can yield high correlations.

The Nov. 12-15, 2016 experiment showed that fluxes gradually increased from section 4 to 1 for all anions, as shown in Figure 2.3. The fluxes of F^-, SO_4^{2-}, and NO_3^- are 42%, 25%, and 55% greater, respectively, on section 1 compared to section 4. However, for the Feb. 17-21, 2017 experiment, fluxes did not necessarily decrease from the leading edge except for NO_3^-; the flux of NO_3^- is just 17% greater on section 1 compared to section 4. The mean hourly wind direction

for both experiments was ~ 210° (SW) with a standard deviation of ~ 90°. Therefore, section 1 was generally the leading edge for both experiments. Observations at one minute resolution from the nearby weather station show that the wind came from the west 49% of the time during Feb. 17-21, 2017 experiment, and therefore the leading edge may have changed such that deposition did not gradually increase in one direction. The presence of large road salt particles may also explain why deposition to section 1 was not necessarily greater than deposition to other sections; these particles can settle through the boundary layer somewhat independently of the boundary layer thickness, which increases with distance from the leading edge as suggested from Figure 2.4.

There is little published information to compare the data from the two experiments on how dry deposition varies over surrogate surfaces under ambient conditions; most experiments have been conducted in wind tunnels with controlled wind speed and direction and turbulence intensity. Under ambient conditions, shifting wind direction can create difficulties in defining the leading edge. However, Raymond et al. (2004) found no difference in deposition of total NO_3^- and SO_4^{2-} onto different positions of the knife-edge surrogate surface in Upstate NY and Maryland. From the current study, the flux varies across the sections of the disk on average by 8% for all anions, suggesting that deposition is relatively uniform even if the height of the boundary layer varies.

2.4 Conclusion

Two identical Teflon-coated disks with a surface area of just over 1 m^2 were designed to measure dry deposition of F^-, Cl^-, SO_4^{2-}, and NO_3^- for short exposures of 2-6 days. Dry deposition fluxes to the two disks agreed well, and computed dry deposition velocities are generally comparable to values measured using smaller surrogate surfaces.

Dry deposition velocities of F^- were in the range 0.6-2.5 cm/s and were slightly greater in summer. On the other hand, dry deposition velocities of Cl^- varied more strongly by season: values in the summer and fall ranged from 1.9 to 2.4 cm/s while values in the winter ranged from 5.5 to 9.2 cm/s. Much of the increase was due to fluxes that increased by a factor of 20 in the winter, while airborne concentrations increased by a smaller amount. It is likely that coarse particles resulting from resuspension of road salt used for deicing are responsible for much of the increase. Dry deposition velocities of SO_4^{2-} also increased in the winter and ranged from 1.1 to 1.8 cm/s, while values in the summer and fall ranged from 0.11 to 0.39 cm/s. Unlike for Cl^-, airborne concentrations did not show a measurable increase compared with the summer and fall, suggesting that an increase in the airborne concentration of coarse particle SO_4^{2-} was enough to increase the flux but had negligible effect on the total airborne concentration, which is mainly submicron.

While dry deposition velocities of Cl^- and SO_4^{2-} were higher in the winter, values of NO_3^- were slightly smaller due to higher airborne concentrations. This may be due to greater formation of NH_4NO_3 in the winter. However, artifacts in sampling NO_3^- with a Teflon filter in the absence of a denuder are likely to reduce the reliability of the NO_3^- airborne concentration data.

On average, dry deposition fluxes to separate sections of the disk varied on average by 8% for all anions in two experiments. This consistency suggests that deposition was approximately uniform despite a changing boundary layer height. Deposition to the first section of the disk, which includes the leading edge, was only slightly enhanced compared with downwind sections.

Chapter 3: Theoretical calculation for washoff of dry deposited SO_4^{2-}

In this chapter, I present a calculation to show if it is possible to quantify the removal of dry deposition from the roof of the War Memorial Arena in downtown Syracuse, NY by measuring the dry deposited mass in the stormwater runoff during a rainstorm. The calculation will be presented for particulate SO_4^{2-}. Two assumptions are made: (1) only dry deposition and the precipitation contribute SO_4^{2-} to the runoff, and (2) all dry deposition is removed within a short time after the rain begins (a time of 10 minutes is assumed). The calculation is possible if the dry deposited mass of SO_4^{2-} appreciably exceeds the mass contributed by the precipitation. If the dry deposited mass of SO_4^{2-} is only a small fraction of the SO_4^{2-} mass in the precipitation, it is likely that the experimental error in determining the small difference between the two concentrations will be too large to quantify accurately.

3.1 Example Calculation

The following parameters are needed: the dry deposition flux of SO_4^{2-} (F), the antecedent dry period during which the flux occurred (ADP), the concentration of SO_4^{2-} in the precipitation (C_P), the surface area of the roof (A), and the rainfall intensity (I). The calculation will assume that ADP = 2.5 days, and I = 2 mm/hr. Removal of dry deposited SO_4^{2-} is likely a first-order process, which means that it will require an infinite time for the mass on the roof to decay to zero. Therefore, another assumption is that nearly all dry deposited SO_4^{2-} is removed within 10 minutes after the storm begins. The time needed to remove nearly all of the dry deposited SO_4^{2-} can be denoted as D = 10 minutes.

On the roof, 14 drains connect to a single drain pipe inside the building where runoff will be sampled. A rough sketch of this area is shown in Figure 3.1; the value of A is 1176 m^2.

The dry deposition flux of SO_4^{2-} for this situation can be computed by using the average value of the dry deposition velocity ($V_{d, ave}$) and the value of the airborne concentration (C_{ave}) for the summer and fall values in Tables 2 and 3 from Chapter 2. Thus, $V_{d, ave}$ equals 0.21 +/- 0.11 cm/s and C_{ave} equals 0.82 +/- 0.58 μg SO_4^{2-} m^{-3}. Therefore, the flux F can be computed as $V_{d, ave}$ x C_{air} = 142 +/- 125 μg SO_4^{2-} m^{-2} day^{-1}. This result is used as a typical value that may be measured in future dry deposition experiments.

To obtain a possible estimate of the SO_4^{2-} precipitation concentration, concentrations from 25 separate measurements during the spring, summer, and fall of 2017 are averaged. For nearly all precipitation events, the concentration of SO_4^{2-} is an average of values from three samples collected during an event (the same analytical and quality control procedures used were the same as those discussed in Chapter 2). The possible value of C_P equals 600 μg SO_4^{2-}/L or 0.6 +/- 0.65 mg SO_4^{2-}/L using these data.

With all parameters known, the calculation can be divided into the following steps (no unit conversions are shown).

Step 1: Calculate the mass of SO_4^{2-} to the roof from dry deposition

The mass that deposits to the roof is F x ADP x A = 142 μg m^2/day x 2.5 days x 1176 m^2 = 417 mg SO_4^{2-}.

Step 2: Calculate the mass of SO_4^{2-} to the roof from the precipitation

The mass contributed by the precipitation is C_P x A x I x D = 600 μg/L x 1176 m^2 x 2 mm/hr x 10 minutes = 240 mg SO_4^{2-}.

The amount from dry deposition exceeds the amount from wet deposition by 177 mg SO_4^{2-}. If the mass from the precipitation is 240 mg SO_4^{2-}, then only an ADP of 1.4 days is required for the amount of dry deposited SO_4^{2-} to equal the amount of SO_4^{2-} contributed by the precipitation during the first 10 minutes of the rainstorm.

Runoff samples collected within the first 10 minutes should have concentrations that exceed the concentration in the precipitation. During this period, runoff concentrations decrease to 0.6 mg SO_4^{2-}/L from an initial concentration, which is calculated below.

Step 3: Calculate the initial concentration of SO_4^{2-} in the runoff

The concentration is the sum of the contributions by dry deposition and the precipitation. The concentration of dry deposited SO_4^{2-} dissolved and suspended in the runoff is equal to the following:

Result from Step 1/(A x I x D) = 417 mg/(1176 m^2 x 2 mm/hr x 10 minutes) = 1.04 mg SO_4^{2-}/L.

Therefore, the average concentration in the runoff within the first 10 minutes of the storm should be 1.04 + 0.6 = 1.64 mg SO_4^{2-}/L. After 10 minutes have passed, the concentration in the runoff should decrease to 0.6 mg SO_4^{2-}/L. This concept is depicted in Figure 3.2. Ideally, the first-order rate constant can be computed using the initial concentration of SO_4^{2-}, the concentration of SO_4^{2-} in the precipitation, and the time it takes for the concentration to decrease to a value close to the level in the precipitation.

Chapter 4: Conclusion and Future Work

In Chapter 2, I presented dry deposition data of F^-, Cl^-, SO_4^{2-}, and NO_3^- for short exposures of 2-6 days using two large disks as surrogate surfaces. Dry deposition fluxes to the two disks agreed well for all anions, and computed dry deposition velocities are comparable to previously published values measured using other surrogate surfaces. Fluxes to separate sections of the disks differ by ~ 8%. These results suggest that the dry deposition data from the disks are reproducible for inorganic anions, and that it may be possible to use the disks to measure other chemical species. Seasonal differences are also apparent, with significantly larger fluxes of SO_4^{2-} and Cl^- observed during the winter possibly due to deposition of deicing salt.

Future work includes the use of two annular denuder systems (URG-2000-30x242-3CSS, URG Corporation, Chapel Hill, NC) to measure airborne concentrations of acid gases such as HF, HCl, SO_2, and HNO_3 during dry deposition experiments. Each denuder is equipped with a Teflon-coated aluminum cyclone to remove coarse particles upstream of the denuder. Analyzing the particles collected in the cyclones will allow for calculation of airborne concentrations of coarse particles, which can be compared to estimates of fine particle concentrations obtained from the Teflon filters downstream of the denuder. A backup nylon filter can quantify evaporated NO_3^- and Cl^- from the Teflon filters, which is not possible with the current setup for airborne concentration measurements. Quantifying any evaporation losses from the filters will help improve airborne concentration measurements and dry deposition velocities of NO_3^- and Cl^-.

Denuders could also be used to provide quantitative evidence of heterogeneous reactions between acid gases (H_4SO_2, HNO_3, organic acids, etc.) and deicing salt. Gases may adsorb to the surface of salt and displace Cl^-, which evaporates as HCl. Measured losses of Cl^- due to

adsorption of acid gases to sea salt aerosol have been quantified in several studies (Saliba and Chamseddine, 2012; Tanner et al., 2001; Yao and Zhang, 2012; Zhuang et al., 1999). This phenomenon may be occurring for deicing salt as well; since road salt aerosol can be abundant during the winter (Kolesar et al., 2018), these reactions may represent an important pathway for acid gases to undergo a change to the particulate phase.

In Chapter 3, I presented an example calculation to show that it may be possible to measure the washoff of dry deposited SO_4^{2-} in the runoff from the roof of the War Memorial Arena in downtown Syracuse, NY. The amount of SO_4^{2-} from dry deposited material dissolved and suspended in the runoff (417 mg) is greater than the amount from the precipitation (240 mg). These calculations assumed an antecedent dry period of 2.5 days and a constant rain intensity of 2 mm/hr. Furthermore, it was assumed that nearly all dry deposited SO_4^{2-} is removed within the first 10 minutes. If this assumption is true, samples collected sequentially at the beginning of the storm will therefore show removal of all dry deposited SO_4^{2-} from the roof. The concentration in the runoff beginning at 10 minutes will remain at the same level as the concentration in the precipitation for the remainder of the storm—a steady state.

Future work includes measuring several dry deposited contaminants in stormwater runoff from the roof of the War Memorial Arena. These experiments will consist of measuring the dry deposition flux during the antecedent dry period, followed by collecting sequential runoff samples simultaneously with collecting precipitation samples. The amount of dry deposited mass will be compared to the mass load in the runoff to determine the removal of dry deposited mass at each time step. This will continue until there is no remaining dry deposited material and a steady state is achieved.

These data will be used to test the assumption of a first order removal process and to derive the first-order rate constant of the removal process for each storm. The rate constant is expected to be dependent on the rain intensity: the rate constant is greater with a higher rain intensity. If the rate constant is small and if the storm is brief, the dry deposited mass may not be completely removed during that storm. But the remaining material may be completely removed in a more intense storm following a second dry period. These hypotheses will be tested in future experiments.

These experiments therefore constitute a new method of estimating dry deposition to urban surfaces by quantifying the removal of dry deposited material in stormwater runoff from these surfaces during a rainstorm. Furthermore, these experiments will assess the relative contributions of dry deposition and wet deposition to contamination of stormwater runoff for various chemical species.

Tables and Figures

Table 2.1: Background information on each experiment. The number of samples collected was the same as the number of field blanks except for 9/5-9/8/16. For the 2/17-2/21/17 experiment, exposure of the air filters began on 2/17 while exposure of the disks began on 2/18. Asterisks denote experiments with the disks divided into sections (see text).

Date	Exposure period (days)	Number of disk samples and blanks	Number of air filters
Sep. 5-8, 2016	3.1	2 samples, 1 blank	0
Oct. 3-7, 2016	3.2	2	1
Oct. 10-12, 2016	2.25	2	2
Nov. 12-15, 2016*	3	3 samples per section, 3 blanks	2
Feb. 17-21, 2017*	3	3 samples per section, 3 blanks	2
Jul. 8-10, 2017	2.1	3	0
Jul. 28-Aug. 30, 2017	5.1	3	4
Aug. 25-30, 2017	5.1	3	4
Sep. 20-26, 2017	6	3	4
Feb. 26-28, 2018	2.1	3	2
Mar. 19-21, 2018	1.9	3	2

Table 2.2: Average dry deposition velocities and standard deviations (both in units of cm/s) of particulate anions for each experiment. If the sample/field blank ratio was below criterion for the airborne concentration or the dry deposition flux, the dry deposition velocity was removed. Standard deviations are compounded based on uncertainties in the samples and in the blanks.

Date	F^-		Cl^-		SO_4^{2-}		NO_3^-	
Summer and Fall	μ_v	σ_v	μ_v	σ_v	μ_v	σ_v	μ_v	σ_v
Oct. 3-7, 2017	1.7	0.4	2.2	0.4	0.12	0.01	0.36	0.04
Oct. 10-12, 2017	1.8	0.2	--	--	0.39	0.04	0.66	0.03
Nov. 12-15, 2017	0.6	0.2	--	--	0.13	0.02	0.10	0.06
Jul. 28- Aug. 2, 2017	0.89	0.2	2.3	0.1	0.21	0.01	1.1	0.06
Aug. 25-30, 2017	1.8	1.2	1.9	0.3	0.27	0.04	0.52	0.12
Sep. 20-26, 2017	2.5	1.1	2.4	1.3	0.11	0.03	0.99	0.28
Winter								
Feb. 17-21, 2017	0.99	0.26	5.5	0.5	1.1	0.09	0.26	0.06
Feb. 26-28, 2018	--	--	9.2	0.5	1.5	0.1	0.41	0.03
Mar. 19-21, 2018	1.0	0.1	7.4	0.9	1.8	0.2	0.15	0.02

Table 2.3: Average airborne concentrations and standard deviations (both in units of $\mu g\ m^{-3}$) of particulate anions for each experiment. If the sample/field blank ratio was below criterion, the value was removed, along with the associated dry deposition velocity in Table 2. Standard deviations are based on uncertainties in the samples and in the blanks.

Date	F^-		Cl^-		SO_4^{2-}		NO_3^-	
Summer and Fall	μ_c	σ_c	μ_c	σ_c	μ_c	σ_c	μ_c	σ_c
Oct. 3-7, 2017	0.0016	0.0002	0.023	0.0007	0.75	0.001	0.69	0.016
Oct. 10-12, 2017	0.001	0.0001	0.012	0.004	0.24	0.014	0.27	0.004
Nov. 12-15, 2017	0.004	0.0006	0.027	0.003	0.81	0.004	0.90	0.006
Jul. 28- Aug. 2, 2017	0.002	0.0003	0.024	0.004	0.74	0.09	0.24	0.03
Aug. 25-30, 2017	0.0007	0.0002	0.053	0.01	0.45	0.051	0.29	0.065
Sep. 20-26, 2017	0.002	0.0007	0.029	0.011	1.9	0.17	0.45	0.04
Winter								
Feb. 17-21, 2017	0.0032	0.0002	1.5	0.065	0.86	0.07	1.0	0.036
Feb. 26-28, 2018	--	--	0.15	0.007	0.59	0.034	0.82	0.03
Mar. 19-21, 2018	0.0036	0.0003	1.2	0.12	0.35	0.01	0.83	0.015

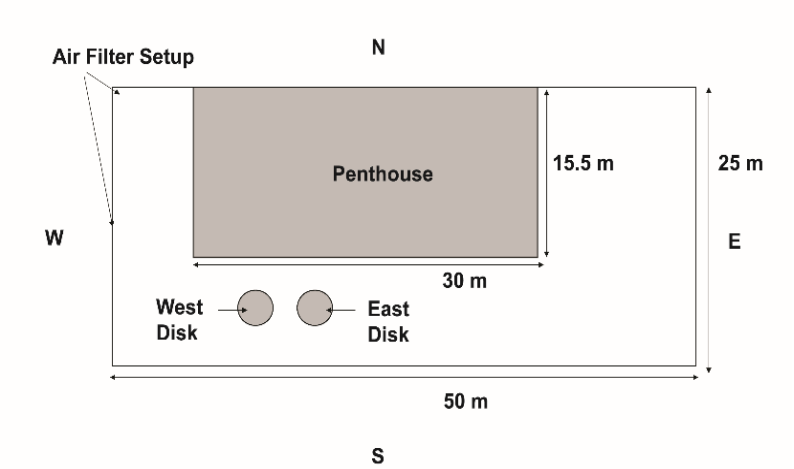

Figure 2.1: Aerial diagram of BRL with roof area dimensions and locations of equipment. The penthouse is on the north side of the roof.

Figure 2.2: The two disks deployed in the field. Each disk is ~ 2.5 m away from the penthouse and the railing. The disks are supported underneath by a frame of PVC pipe secured to concrete pavers.

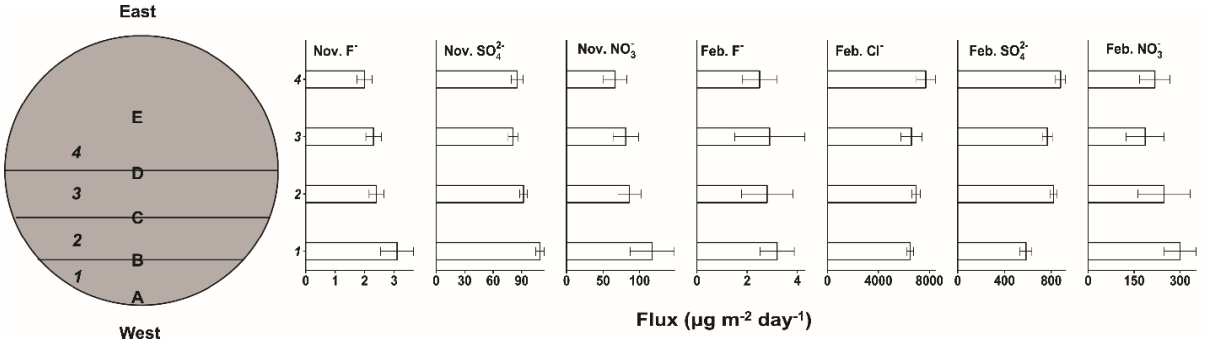

Figure 2.3: (Right) Average fluxes to each section shown in the graph on the right. Standard deviations are included as error bars; (Left) Sections are numbered in increasing order from W-E with section 1 assigned the leading edge. Velocity profiles are calculated at positions A, B, C, D, and E along the surface of the disks, which are shown in Figure 4.

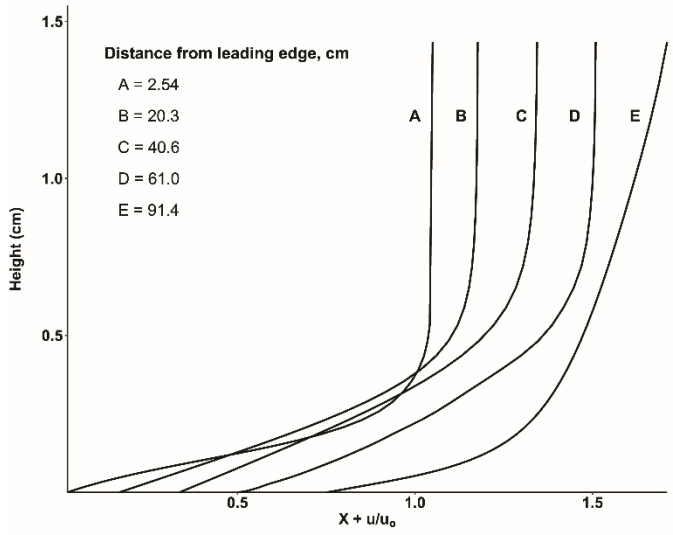

Figure 2.4: Velocity profiles computed at five positions along the surface of the disks. The x-axis is normalized by height and distance in the x-direction, where X = distance from leading edge/diameter of disk and u/u_o = velocity/3 (the inlet velocity is 3 m/s).

Figure 3.1: Aerial view of traditional roof on War Memorial building in downtown Syracuse, NY. The area of the roof that drains to the sampling pipes is indicated in the black box. This area is 1176 m^2, measured using CAD by Onondaga County staff.

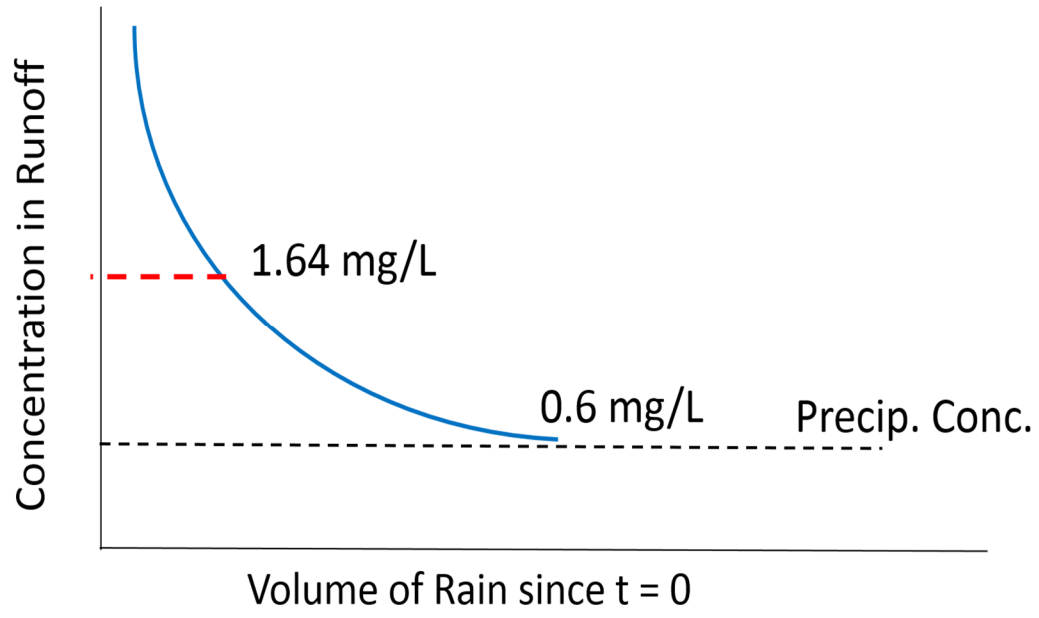

Figure 3.2: Washoff of dry deposited SO_4^{2-} from the roof on the War Memorial. The initial concentration of 1.64 mg SO_4^{2-}/L in the runoff decreases to the concentration of 0.6 mg SO_4^{2-}/L found in the precipitation, which remains at steady-state for the remainder of the storm.

Appendix

Table A.1: Dry Deposition Fluxes

Date	Flux (μg m^{-2} day^{-1})	Disk	Anion	Exposure (days)
10/3-10/7/16	45.6	West	Cl	3.20
10/3-10/7/16	41.4	East	Cl	3.20
2/17-2/21/17	6972.9	West	Cl	3.00
2/17-2/21/17	7359.7	East	Cl	3.00
7/8-7/10/17	39.1	West	Cl	2.08
7/8-7/10/17	29.3	East	Cl	2.08
7/28-8/2/17	47.4	East	Cl	5.10
8/25-8/30/17	67.5	East	Cl	5.07
8/25-8/30/17	70.6	West	Cl	5.07
9/20-9/26/17	55.2	East	Cl	5.96
9/20-9/26/17	65.4	West	Cl	5.96
2/26-2/28/18	1226.0	West	Cl	2.07
2/26-2/28/18	1176.7	East	Cl	2.07
3/19-3/21/18	7351.2	West	Cl	1.90
3/19-3/21/18	7715.6	East	Cl	1.90
9/5-9/8/16	0.5	West	F	3.08
9/5-9/8/16	0.4	East	F	3.08
10/3-10/7/16	2.2	West	F	3.20
10/3-10/7/16	2.1	East	F	3.20
10/10-10/12/16	1.5	West	F	2.25
10/10-10/12/16	1.5	East	F	2.25
11/12-11/15/16	2.3	West	F	3.00
11/12-11/15/16	2.4	East	F	3.00
2/17-2/21/17	2.8	West	F	3.00
2/17-2/21/17	2.6	East	F	3.00
7/8-7/10/17	2.1	West	F	2.08
7/8-7/10/17	2.0	East	F	2.08
7/28-8/2/17	1.6	East	F	5.10
8/25-8/30/17	2.2	West	F	5.07
8/25-8/30/17	2.1	East	F	5.07
9/20-9/26/17	4.2	West	F	5.96
9/20-9/26/17	4.4	East	F	5.96
2/26-2/28/18	2.5	West	F	2.07
2/26-2/28/18	2.7	East	F	2.07
3/19-3/21/18	3.4	West	F	1.90
3/19-3/21/18	3.1	East	F	1.90
10/3-10/7/16	191.5	East	NO3	3.20
10/3-10/7/16	230.0	West	NO3	3.20
10/10-10/12/16	154.7	East	NO3	2.25
10/10-10/12/16	150.5	West	NO3	2.25

11/12-11/15/16	92.2	West	NO3	3.00
11/12-11/15/16	101.6	East	NO3	3.00
2/17-2/21/17	215.5	West	NO3	3.00
2/17-2/21/17	232.0	East	NO3	3.00
7/28-8/2/17	227.7	East	NO3	5.10
8/25-8/30/17	128.7	East	NO3	5.07
8/25-8/30/17	136.5	West	NO3	5.07
9/20-9/26/17	383.1	East	NO3	5.96
9/20-9/26/17	379.6	West	NO3	5.96
2/26-2/28/18	279.2	West	NO3	2.07
2/26-2/28/18	294.3	East	NO3	2.07
3/19-3/21/18	109.4	West	NO3	1.90
3/19-3/21/18	110.3	East	NO3	1.90
9/5-9/8/16	87.8	West	SO4	3.08
9/5-9/8/16	76.3	East	SO4	3.08
10/3-10/7/16	83.3	West	SO4	3.20
10/3-10/7/16	71.1	East	SO4	3.20
10/10-10/12/16	77.8	West	SO4	2.25
10/10-10/12/16	80.9	East	SO4	2.25
11/12-11/15/16	85.4	West	SO4	3.00
11/12-11/15/16	90.0	East	SO4	3.00
2/17-2/21/17	800.7	West	SO4	3.00
2/17-2/21/17	820.4	East	SO4	3.00
7/8-7/10/17	67.4	West	SO4	2.08
7/8-7/10/17	79.3	East	SO4	2.08
7/28-8/2/17	133.7	East	SO4	5.10
8/25-8/30/17	104.7	West	SO4	5.07
8/25-8/30/17	103.1	East	SO4	5.07
9/20-9/26/17	184.2	West	SO4	5.96
9/20-9/26/17	179.0	East	SO4	5.96
2/26-2/28/18	732.3	West	SO4	2.07
2/26-2/28/18	796.6	East	SO4	2.07
3/19-3/21/18	586.0	West	SO4	1.90
3/19-3/21/18	507.9	East	SO4	1.90

Note: the above data were imported into R to conduct Wilcoxon rank-sum tests for each anion: West vs. East. The tests failed to reject the null hypothesis for all anions ($p>>0.05$). Fluxes are reported as $\mu g\ F^{-}\ m^{-2}\ day^{-1}$, $\mu g\ Cl^{-}\ m^{-2}\ day^{-1}$, $\mu g\ SO_4^{2-}\ m^{-2}\ day^{-1}$, and $\mu g\ NO_3^{-}\ m^{-2}\ day^{-1}$

Table A.2: Airborne Concentrations

Date	Airborne Concentration	Flow Meter	Anion
10/3-10/7/16	0.002	FR1	F
10/3-10/7/16	0.023	FR1	Cl
10/3-10/7/16	0.753	FR1	SO4
10/3-10/7/16	0.679	FR1	NO3
10/10-10/12/16	0.0009	FR1	F
10/10-10/12/16	0.0010	FR2	F
10/10-10/12/16	0.014	FR1	Cl
10/10-10/12/16	0.009	FR2	Cl
10/10-10/12/16	0.244	FR1	SO4
10/10-10/12/16	0.232	FR2	SO4
10/10-10/12/16	0.262	FR1	NO3
10/10-10/12/16	0.271	FR2	NO3
11/12-11/15/16	0.004	FR1	F
11/12-11/15/16	0.004	FR2	F
11/12-11/15/16	0.027	FR1	Cl
11/12-11/15/16	0.023	FR2	Cl
11/12-11/15/16	0.806	FR1	SO4
11/12-11/15/16	0.809	FR2	SO4
11/12-11/15/16	0.903	FR1	NO3
11/12-11/15/16	0.895	FR2	NO3
2/17-2/21/17	0.003	FR1	F
2/17-2/21/17	0.003	FR2	F
2/17-2/21/17	1.586	FR1	Cl
2/17-2/21/17	1.456	FR2	Cl
2/17-2/21/17	0.860	FR1	SO4
2/17-2/21/17	0.789	FR2	SO4
2/17-2/21/17	1.013	FR1	NO3
2/17-2/21/17	1.059	FR2	NO3
7/28-8/2/17	0.003	FR1	F
7/28-8/2/17	0.002	FR2	F
7/28-8/2/17	0.002	FL1	F
7/28-8/2/17	0.001	FL2	F
7/28-8/2/17	0.026	FR1	Cl
7/28-8/2/17	0.024	FR2	Cl
7/28-8/2/17	0.021	FL1	Cl
7/28-8/2/17	0.025	FL2	Cl
7/28-8/2/17	0.787	FR1	SO4
7/28-8/2/17	0.802	FR2	SO4
7/28-8/2/17	0.672	FL1	SO4

7/28-8/2/17	0.713	FL2	SO4
7/28-8/2/17	0.258	FR1	NO3
7/28-8/2/17	0.260	FR2	NO3
7/28-8/2/17	0.202	FL1	NO3
7/28-8/2/17	0.239	FL2	NO3
8/25-8/30/17	0.0006	FR1	F
8/25-8/30/17	0.0007	FR2	F
8/25-8/30/17	0.0007	FL1	F
8/25-8/30/17	0.0007	FL2	F
8/25-8/30/17	0.056	FR1	Cl
8/25-8/30/17	0.053	FR2	Cl
8/25-8/30/17	0.054	FL1	Cl
8/25-8/30/17	0.050	FL2	Cl
8/25-8/30/17	0.480	FR1	SO4
8/25-8/30/17	0.494	FR2	SO4
8/25-8/30/17	0.409	FL1	SO4
8/25-8/30/17	0.408	FL2	SO4
8/25-8/30/17	0.298	FR1	NO3
8/25-8/30/17	0.383	FR2	NO3
8/25-8/30/17	0.242	FL1	NO3
8/25-8/30/17	0.248	FL2	NO3
9/20-9/26/17	0.0025	FR1	F
9/20-9/26/17	0.0021	FR2	F
9/20-9/26/17	0.0024	FL1	F
9/20-9/26/17	0.0010	FL2	F
9/20-9/26/17	0.024	FR1	Cl
9/20-9/26/17	0.020	FR2	Cl
9/20-9/26/17	0.024	FL1	Cl
9/20-9/26/17	0.045	FL2	Cl
9/20-9/26/17	1.947	FR1	SO4
9/20-9/26/17	1.967	FR2	SO4
9/20-9/26/17	1.903	FL1	SO4
9/20-9/26/17	1.837	FL2	SO4
9/20-9/26/17	0.481	FR1	NO3
9/20-9/26/17	0.411	FR2	NO3
9/20-9/26/17	0.457	FL1	NO3
9/20-9/26/17	0.433	FL2	NO3
2/26-2/28/18	0.0012	FR1	F
2/26-2/28/18	0.0010	FR2	F
2/26-2/28/18	0.157	FR1	Cl
2/26-2/28/18	0.144	FR2	Cl

2/26-2/28/18	0.626	FR1	SO4
2/26-2/28/18	0.557	FR2	SO4
2/26-2/28/18	0.809	FR1	NO3
2/26-2/28/18	0.821	FR2	NO3
3/19-3/21/18	0.0038	FR1	F
3/19-3/21/18	0.0033	FR2	F
3/19-3/21/18	1.287	FR1	Cl
3/19-3/21/18	1.065	FR2	Cl
3/19-3/21/18	0.364	FR1	SO4
3/19-3/21/18	0.344	FR2	SO4
3/19-3/21/18	0.836	FR1	NO3
3/19-3/21/18	0.826	FR2	NO3

Note: airborne concentrations of inorganic anions expressed as μg F^- m^{-3}, μg Cl^- m^{-3}, μg SO_4^{2-} m^{-3}, and μg NO_3^- m^{-3}. During sampling, each filter was connected to a flow meter designated FR1, FR2, FL1, or FL2. The airborne concentrations were averaged for each anion and experiment to obtain the values in Table 2.3.

Table A.3: East-West Flux Differences

Experiment Date	F	Cl	SO4	NO3
9/5-9/8/16	0.0937	NA	0.1395	NA
10/3-10/7/16	0.1867	0.0959	0.1589	0.1824
10/10-10/12/16	0.0332	NA	0.0391	0.0280
11/12-11/15/16	0.0677	0.0045	0.0517	0.1222
2/17-2/21/17	0.0426	0.0540	0.0236	0.0738
7/8-7/10/17	0.0154	0.2880	0.1627	NA
7/28-8/2/17	NA	NA	NA	NA
8/25-8/30/17	0.0613	0.0446	0.0153	0.0586
9/20-9/26/17	0.0384	0.1696	0.0287	0.0089
2/26-2/26/18	0.0909	0.0410	0.0841	0.0528
3/19-3/21/18	0.0915	0.0484	0.1429	0.0080
AVE	0.0721	0.0933	0.0846	0.0669
Grand Average	0.0791			

Note: the formula used to compute the difference between the flux to the east disk and the flux to the west disk was ABS((X1-X2)/(0.5*(X1+X2))) where X1 = flux from west disk and X2 = flux from east disk. The values reported in the table are therefore expressed as fractions of the average of the 2 values. Multiplying each value by 100 yields the percent difference. The differences for each anion were then averaged. The percent differences of these values are included in Chapter 2. The Grand Average is an average of all values in the table.

Table A.4: Disk Sample/Blank Ratios					
S/B		F	Cl	SO4	NO3
9/5-9/8/16		7.40	2.90	8.70	1.71
10/3-10/7/16		16.00	12.60	29.20	22.60
10/10-10/12/16		6.60	1.86	9.80	11.60
11/12-11/15/16		9.47	4.29	13.08	6.40
2/17-2/21/17		14.25	92.75	137.15	17.06
7/8-7/10/17		24.00	14.70	28.20	2.93
7/28-8/2/17		14.70	26.70	54.90	24.00
8/25-8/30/17		19.50	45.90	47.70	40.50
9/20-9/26/17		14.40	10.20	13.50	15.60
2/26-2/26/18		12.60	117.30	45.00	29.70
3/19-3/21/18		18.97	58.83	44.58	24.05
	Average	14.35	35.28	39.25	17.83
				Grand Ave	26.68

Table A.5: Air Filter Sample/Blank Ratios				
S/B	F	Cl	SO4	NO3
10/3-10/7/16	Inf	32.25	561.97	78.30
10/10-10/12/16	12.28	Inf	Inf	134.17
11/12-11/15/16	15.11	18.21	590.15	86.41
2/17-2/21/17	34.00	776.98	166.61	48.12
7/8-7/10/17	1.72	2.97	157.39	2.31
7/28-8/2/17	29.58	68.41	1428.45	43.82
8/25-8/30/17	8.54	Inf	Inf	69.91
9/20-9/26/17	220.20	54.28	3216.81	76.74
2/26-2/26/18	2.13	Inf	20.14	25.93
3/19-3/21/18	5.02	99.02	27.01	45.73

Note: For Table A.4 and Table A.5, values highlighted in yellow indicate S/B ratios <5. A value of "Inf" means that the S/B = infinity because all field blanks were below detection limits and were set equal to zero.

Table A.6: Avg. Disk Blank compared to Sample 3

Date	Sample Type	Anion	Mass (µg)
9/5-9/8/16	West3	F	0.18
9/5-9/8/16	East3	F	0.20
9/5-9/8/16	Blank	F	0.30
9/5-9/8/16	West3	SO4	38.26
9/5-9/8/16	East3	SO4	30.95
9/5-9/8/16	Blank	SO4	43.86
9/5-9/8/16	West3	Cl	NA
9/5-9/8/16	East3	Cl	NA
9/5-9/8/16	Blank	Cl	NA
9/5-9/8/16	West3	NO3	NA
9/5-9/8/16	East3	NO3	NA
9/5-9/8/16	Blank	NO3	NA
10/3-10/7/16	West3	F	1.59
10/3-10/7/16	East3	F	1.25
10/3-10/7/16	Blank	F	0.66
10/3-10/7/16	Blank	Cl	15.23
10/3-10/7/16	West3	Cl	15.01
10/3-10/7/16	East3	Cl	23.25
10/3-10/7/16	Blank	SO4	10.47
10/3-10/7/16	West3	SO4	24.98
10/3-10/7/16	East3	SO4	22.07
10/3-10/7/16	Blank	NO3	37.72
10/3-10/7/16	West3	NO3	65.59
10/3-10/7/16	East3	NO3	48.51
10/10-10/12/16	Blank	F	0.79
10/10-10/12/16	West3	F	0.96
10/10-10/12/16	East3	F	1.05
10/10-10/12/16	Blank	Cl	NA
10/10-10/12/16	West3	Cl	NA
10/10-10/12/16	East3	Cl	NA
10/10-10/12/16	Blank	SO4	25.03
10/10-10/12/16	West3	SO4	17.83
10/10-10/12/16	East3	SO4	22.93
10/10-10/12/16	Blank	NO3	39.62
10/10-10/12/16	West3	NO3	46.08
10/10-10/12/16	East3	NO3	56.76
11/12-11/15/16	Blank	F	1.12
11/12-11/15/16	West3	F	1.35
11/12-11/15/16	East3	F	1.17

11/12-11/15/16	Blank	Cl	NA
11/12-11/15/16	West3	Cl	NA
11/12-11/15/16	East3	Cl	NA
11/12-11/15/16	Blank	SO4	30.24
11/12-11/15/16	West3	SO4	28.08
11/12-11/15/16	East3	SO4	13.85
11/12-11/15/16	Blank	NO3	58.15
11/12-11/15/16	West3	NO3	52.42
11/12-11/15/16	East3	NO3	47.37
2/17-2/21/17	Blank	F	0.83
2/17-2/21/17	West3	F	0.64
2/17-2/21/17	East3	F	1.15
2/17-2/21/17	Blank	Cl	275.71
2/17-2/21/17	West3	Cl	607.58
2/17-2/21/17	East3	Cl	1527.05
2/17-2/21/17	Blank	SO4	20.86
2/17-2/21/17	West3	SO4	95.07
2/17-2/21/17	East3	SO4	214.98
2/17-2/21/17	Blank	NO3	54.95
2/17-2/21/17	West3	NO3	39.41
2/17-2/21/17	East3	NO3	150.28
7/8-7/10/17	Blank	F	0.23
7/8-7/10/17	West3	F	0.49
7/8-7/10/17	East3	F	0.47
7/8-7/10/17	Blank	Cl	7.05
7/8-7/10/17	West3	Cl	5.01
7/8-7/10/17	East3	Cl	4.77
7/8-7/10/17	Blank	SO4	6.96
7/8-7/10/17	West3	SO4	6.32
7/8-7/10/17	East3	SO4	7.16
7/8-7/10/17	Blank	NO3	35.35
7/8-7/10/17	West3	NO3	22.26
7/8-7/10/17	East3	NO3	10.56
7/28-8/2/17	Blank	F	0.64
7/28-8/2/17	West3	F	NA
7/28-8/2/17	East3	F	0.84
7/28-8/2/17	Blank	Cl	8.58
7/28-8/2/17	West3	Cl	NA
7/28-8/2/17	East3	Cl	9.37
7/28-8/2/17	Blank	SO4	11.64
7/28-8/2/17	West3	SO4	NA

7/28-8/2/17	East3	SO4	44.15
7/28-8/2/17	Blank	NO3	48.09
7/28-8/2/17	West3	NO3	NA
7/28-8/2/17	East3	NO3	57.04
8/25-8/30/17	Blank	F	0.76
8/25-8/30/17	West3	F	0.93
8/25-8/30/17	East3	F	1.17
8/25-8/30/17	Blank	Cl	9.47
8/25-8/30/17	West3	Cl	7.99
8/25-8/30/17	East3	Cl	10.01
8/25-8/30/17	Blank	SO4	13.57
8/25-8/30/17	West3	SO4	15.68
8/25-8/30/17	East3	SO4	18.43
8/25-8/30/17	Blank	NO3	20.78
8/25-8/30/17	West3	NO3	17.95
8/25-8/30/17	East3	NO3	32.18
9/20-9/26/17	Blank	F	2.56
9/20-9/26/17	West3	F	2.14
9/20-9/26/17	East3	F	2.09
9/20-9/26/17	Blank	Cl	57.60
9/20-9/26/17	West3	Cl	103.34
9/20-9/26/17	East3	Cl	47.57
9/20-9/26/17	Blank	SO4	120.82
9/20-9/26/17	West3	SO4	53.92
9/20-9/26/17	East3	SO4	52.77
9/20-9/26/17	Blank	NO3	210.76
9/20-9/26/17	West3	NO3	52.20
9/20-9/26/17	East3	NO3	58.49
2/26-2/28/18	Blank	F	0.65
2/26-2/28/18	West3	F	0.81
2/26-2/28/18	East3	F	1.14
2/26-2/28/18	Blank	Cl	25.16
2/26-2/28/18	West3	Cl	51.60
2/26-2/28/18	East3	Cl	89.39
2/26-2/28/18	Blank	SO4	43.45
2/26-2/28/18	West3	SO4	63.53
2/26-2/28/18	East3	SO4	160.01
2/26-2/28/18	Blank	NO3	25.72
2/26-2/28/18	West3	NO3	31.41
2/26-2/28/18	East3	NO3	48.62
3/19-3/21/18	Blank	F	0.44

3/19-3/21/18	West3	F	0.83
3/19-3/21/18	East3	F	0.77
3/19-3/21/18	Blank	Cl	296.14
3/19-3/21/18	West3	Cl	469.01
3/19-3/21/18	East3	Cl	501.23
3/19-3/21/18	Blank	SO4	28.83
3/19-3/21/18	West3	SO4	66.32
3/19-3/21/18	East3	SO4	61.25
3/19-3/21/18	Blank	NO3	11.45
3/19-3/21/18	West3	NO3	7.81
3/19-3/21/18	East3	NO3	10.25

Note: order of "Sample Type" changes but has no effect on calculations in R. A value for the sample type "Blank" is the average mass in the blanks (computed as average of the 6 blanks from both disks); a value for "West3" is the mass in the third (or final) sample collected from the west disk; and a value for "East3" is the mass in the third (or final) sample collected from the east disk. The masses are expressed as μg F^-, μg Cl^-, μg SO_4^{2-}, and μg NO_3^-.

In R, pairwise Wilcoxon signed-rank tests were conducted for each anion: Blank vs. West3 and Blank vs. East3. The tests were conducted with and without Bonferroni corrections; both tests failed to reject the null hypothesis for all anions ($p>0.05$).

Table A.7: Fraction of Mass in first sample (each sample is blank corrected)

Experiment Date	F		Cl		SO4		NO3	
	W	E	W	E	W	E	W	E
9/5-9/8/16	1.00	1.00	1.00	1.00	1.00	1.00	NA	NA
10/3-10/7/16	0.91	0.93	1.00	0.95	0.95	0.96	0.97	0.98
10/10-10/12/16	0.95	0.93	NA	NA	1.00	1.00	0.98	0.96
11/12-11/15/16	0.89	0.93	NA	NA	0.96	1.00	1.00	1.00
2/17-2/21/17	0.98	0.85	0.95	0.90	0.91	0.85	1.00	0.87
7/8-7/10/17	0.85	0.91	0.99	1.00	0.97	0.97	NA	NA
7/28-8/2/17	NA	0.87	NA	0.93	NA	0.83	NA	0.91
8/25-8/30/17	0.93	0.87	0.99	0.96	0.95	0.93	0.99	0.94
9/20-9/26/17	0.98	0.87	0.97	1.00	1.00	1.00	1.00	1.00
2/26-2/26/18	0.89	0.79	0.93	0.90	0.90	0.82	0.94	0.85
3/19-3/21/18	0.82	0.83	0.95	0.94	0.91	0.87	0.98	0.96

Analyte	F		Cl		SO4		NO3	
Disk	W1	E1	W1	E1	W1	E1	W1	E1
μ	0.92	0.89	0.97	0.97	0.96	0.94	1.00	0.97
Median	0.92	0.87	0.98	0.95	0.96	0.96	0.99	0.96
σ	0.059	0.057	0.026	0.061	0.048	0.085	0.074	0.099
Average of W1, E1	0.90		0.97		0.95		0.99	

Note: Each value is the fraction of the total mass deposited to each disk in the first sample. On average, the volume of sample 1 comprises 41% of the total volume in all three samples collected from each disk.

Table A.8: Analytical Detection Limits

Date-F	μ	σ	LOD	LOQ	Date-Cl	μ	σ	LOD	LOQ
161010	0.016	0.019	0.073	0.206	161010	0.038	0.010	0.069	0.140
161026	0.035	0.013	0.073	0.160	161026	0.053	0.054	0.216	0.595
161116	0.023	0.010	0.031	0.102	161116	0.050	0.036	0.109	0.363
161202	0.102	0.002	0.109	0.124	161202	0.021	0.005	0.036	0.070
161209	0.008	0.001	0.011	0.019	161209	0.047	0.023	0.115	0.273
161212	0.004	0.004	0.013	0.043	161212	0.039	0.010	0.030	0.101
170301	0.003	0.002	0.008	0.019	170301	0.235	0.015	0.279	0.382
170308	0.09	0.017	0.140	0.257	170308	0.047	0.006	0.065	0.105
170728	0.011	0.006	0.027	0.066	170728	0.065	0.050	0.216	0.568
170805	0.041	0.022	0.106	0.259	170805	0.083	0.037	0.194	0.451
170808	0.016	0.011	0.048	0.121	170808	0.044	0.010	0.074	0.143
170923	0.063	0.024	0.135	0.303	170923	0.075	0.045	0.211	0.529
171006	0.006	0.003	0.015	0.037	171006	0.027	0.004	0.040	0.071
171007	0.011	0.005	0.027	0.064	171007	0.026	0.004	0.037	0.064
171008	0.007	0.002	0.015	0.031	171008	0.026	0.005	0.040	0.073
180303	0.195	0.001	0.198	0.206	180303	0.685	0.086	0.942	1.541
180326	0.088	0.003	0.097	0.120	180326	0.062	0.023	0.131	0.290

Date-SO4	μ	σ	LOD	LOQ	Date-NO3	μ	σ	LOD	LOQ
161010	0.034	0.008	0.057	0.111	161010	0.014	0.008	0.037	0.090
161026	0.013	0.011	0.047	0.126	161026	1.813	0.006	1.832	1.876
161116	0.015	0.011	0.032	0.106	161116	0.025	0.012	0.035	0.116
161202	0.003	0.002	0.008	0.021	161202	2.210	0.000	2.210	2.211
161209	0.017	0.006	0.035	0.078	161209	0.033	0.009	0.059	0.122
161212	0.017	0.004	0.013	0.045	161212	0.009	0.007	0.021	0.069
170301	0.182	0.045	0.315	0.627	170301	0.362	0.026	0.439	0.619
170308	8E-04	0.001	0.003	0.007	170308	0.001	0.001	0.003	0.007
170728	0.034	0.023	0.102	0.262	170728	0.037	0.039	0.154	0.426
170805	0.12	0.021	0.183	0.331	170805	0.064	0.013	0.103	0.194
170808	0.088	0.029	0.175	0.378	170808	0.034	0.014	0.075	0.171
170923	0.039	0.023	0.109	0.273	170923	0.064	0.040	0.184	0.463
171006	0.008	0.003	0.018	0.040	171006	0.001	0.001	0.004	0.010
171007	0.013	0.003	0.023	0.048	171007	0.003	0.001	0.006	0.013
171008	0.012	0.003	0.022	0.045	171008	0.001	0.000	0.002	0.005
180303	0.035	0.018	0.089	0.216	180303	1.049	0.038	1.163	1.429
180326	0.048	0.015	0.094	0.202	180326	0.035	0.023	0.102	0.260

Note: Calculations for each analytical run were computed using the mean and standard deviation of concentrations (in μmol/L) of 10 water blanks ran immediately after each calibration. The date of the run is listed as "YYMMDD" where YY = year, MM = month, and DD = day.

Table A.9: SO_4^{2-} Precipitation Concentrations

Date	# samples	C_{ave} (μg/L)
4/4/2017	3	314.0
4/15/2017	1	2142.1
6/4/17 (Period 1)	3	366.7
6/4/17 (Period 2)	3	154.0
6/4/17 (Period 3)	3	579.0
6/4/17 (Period 4)	3	674.3
6/4/17 (Period 5)	3	537.9
6/4/17 (Period 6)	3	756.9
6/4/17 (Period 7)	3	1201.5
6/6/17 (Period 1)	3	45.7
6/6/17 (Period 2)	3	75.0
7/10/2017	3	611.5
7/12/17 (Period 1)	3	754.6
7/12/17 (Period 2)	3	261.1
7/13/17 (Period 1)	3	84.2
7/13/17 (Period 2)	3	226.9
7/20/2017	3	867.4
8/3/2017	1	2863.2
8/4/2017 (Period 1)	2	380.1
8/4/17 (Period 2)	2	398.2
9/2/17 (Period 1)	3	177.8
9/2/17 (Period 2)	3	42.6
9/3/17 (Period 1)	3	618.6
9/29/2017	3	728.1
10/9/2017	3	93.4
	Average	598
	Standard Deviation	654.5

Note: These values are precipitation concentrations of SO_4^{2-} (expressed as μg SO_4^{2-}/L) for 25 separate sets of samples. Some samples were collected during the same storm but in separate intervals—these are designated as "Period 1," "Period 2," etc. In general, the value reported in the third column is an average of 3 samples, and the standard deviation of each value is much smaller than the average.

Standard deviation of the dry deposition velocity

Error propagation is used to derive the standard deviation of the dry deposition flux, the standard deviation of the airborne concentration, and the standard deviation of the dry deposition velocity. For example, the uncertainty in the standard deviation of the dry deposition velocity is a function of the uncertainties of the flux and the airborne concentration:

$$\sigma_v^2 = \left(\frac{\partial V}{\partial F}\right)^2 \sigma_F^2 + \left(\frac{\partial V}{\partial c}\right)^2 \sigma_c^2$$

where σ_v = standard deviation of the deposition velocity, σ_F = standard deviation of the flux, σ_c = standard deviation of the airborne concentration. The standard deviation of the dry deposition velocity is therefore:

$$\sigma_v = \sqrt{\frac{\sigma_F^2}{\mu_c^2} + \frac{\mu_F^2 \sigma_c^2}{\mu_c^4}}$$

where μ_F = average flux, μ_c = average airborne concentration, and all σ terms are the same as above.

References

https://www.epa.gov/castnet. Accessed Aug. 7, 2018.

http://www.ncdc.noaa.gov. Accessed Jun. 17, 2018.

A. Sehmel, G., 1980. Particle and gas dry deposition: a review, Atmos. Environ. (1967). https://doi.org/10.1016/0004-6981(80)90031-1

Aftab, S.M.A., Rafie, A.S.M., Razak, N.A., Ahmad, K.A., 2016. Turbulence model selection for low reynolds number flows. PLoS One 11, 1–15. https://doi.org/10.1371/journal.pone.0153755

Anwar Hossain, K.M., Easa, S.M., Lachemi, M., 2009. Evaluation of the effect of marine salts on urban built infrastructure. Build. Environ. 44, 713–722. https://doi.org/10.1016/j.buildenv.2008.06.004

Ban, S., Matsuda, K., Sato, K., Ohizumi, T., 2016. Long-term assessment of nitrogen deposition at remote EANET sites in Japan. Atmos. Environ. 146, 70–78.

Bonazza, A., Brimblecombe, P., Grossi, C.M., Sabbioni, C., 2007. Carbon in black crusts from the Tower of London. Environ. Sci. Technol. 41, 4199–4204. https://doi.org/10.1021/es062417w

Boyle, E.A., Lee, J.-M., Echegoyen, Y., Noble, A., Moos, S., Carrasco, G., Zhao, N., Kayser, R., Zhang, J., Gamo, T., Obata, H., Norisuye, K., 2014. Anthropogenic lead emissions in the ocean. Oceanography 27, 69–75.

Bozlaker, A., Muezzinoglu, A., Odabasi, M., 2008. Atmospheric concentrations, dry deposition and air–soil exchange of polycyclic aromatic hydrocarbons (PAHs) in an industrial region in Turkey 153, 1093–1102. https://doi.org/10.1016/j.jhazmat.2007.09.064

Carpman, N., 2011. Turbulence Intensity in Complex Environments and its Influence on Small

Wind Turbines. Dept. Earth Sci. Uppsala Univ.

Chan, E.A.W., Gantt, B., McDow, S., 2018. The reduction of summer sulfate and switch from summertime to wintertime $PM_{2.5}$ concentration maxima in the United States. Atmos. Environ. 175, 25–32. https://doi.org/10.1016/j.atmosenv.2017.11.055

Chang, K., Fang, G., Lu, C., Bai, H., 2003. Estimating PAH dry deposition by measuring gas and particle phase concentrations in ambient air 3, Aerosol Air Qual. Res. 41–51.

Chen, S., Fang, G., Lin, C., Hsieh, L., 1996. Dry deposition and particle size distributions of nitrate and sulfate in ambient air. Toxicol. Environ. Chem. 62, 49–64. https://doi.org/10.1080/02772249709358497

Chien, C., Ho, T., Sanborn, M.E., Yin, Q., Paytan, A., 2017. Lead concentrations and isotopic compositions in the Western Philippine Sea. Mar. Chem. 189, 10–16. https://doi.org/10.1016/j.marchem.2016.12.007

Chu, C.C., Fang, G.C., Chen, J.C., Yang, I.L., 2008. Dry deposition study by using dry deposition plate and water surface sampler in Shalu, central Taiwan. Environ. Monit. Assess. 146, 441–451. https://doi.org/10.1007/s10661-007-0090-8

Dasch, J.M., 1985. Direct measurement of dry deposition to a polyethylene bucket and various surrogate surfaces. Environ. Sci. Technol. 19, 721–725. https://doi.org/10.1021/es00138a011

Davidson, C.I., Lindberg, S.E., Schmidt, J.A., Cartwright, L.G., Landis, L.R., 1985. Dry deposition of sulfate onto surrogate surfaces. J. Geophys. Res. 90, 2123–2130. https://doi.org/10.1029/JD090iD01p02123

Driscoll, C.T., Lawrence, G.B., Bulger, A.J., Butler, T.J., Cronan, C.S., Eagar, C., Lambert, K.F.,

Likens, G.E., Stoddard, J.L., Weathers, K.C., 2018. Acidic deposition in the Northeastern United States: sources and inputs, ecosystem effects, and management strategies. Bioscience 51, 180–198.

Endo, T., Yagoh, H., Sato, K., Matsuda, K., Hayashi, K., Noguchi, I., Sawada, K., 2011. Regional characteristics of dry deposition of sulfur and nitrogen compounds at EANET sites in Japan from 2003 to 2008. Atmos. Environ. 45, 1259–1267. https://doi.org/10.1016/j.atmosenv.2010.12.003

Eng, A., Harner, T., Pozo, K., 2013. A prototype passive air sampler for measuring dry deposition of polycyclic aromatic hydrocarbons. Environ. Sci. Technol. Lett. 1, 77–81. https://doi.org/10.1021/ez400044z

Erisman, J.W., Van Pul, A., Wyers, P., 1994. Parametrization of surface resistance for the quantification of atmospheric deposition of acidifying pollutants and ozone. Atmos. Environ. 28, 2595–2607. https://doi.org/https://doi.org/10.1016/1352-2310(94)90433-2

Etyemezian, V., Davidson, C.I., Finger, S., Striegel, M.F., Barabas, N., Chow, J.C., 1998. Vertical gradients of pollutant concentrations and deposition fluxes on a tall limestone building. J. Am. Inst. Conserv. 37, 187–210. https://doi.org/10.2307/3179802

Fishwick, M.P., Ussher, S.J., Sedwick, P.N., Lohan, M.C., Worsfold, P.J., Buck, K.N., Church, T.M., 2018. Impact of surface ocean conditions and aerosol provenance on the dissolution of aerosol manganese, cobalt, nickel and lead in seawater. Mar. Chem. 198, 28–43. https://doi.org/10.1016/j.marchem.2017.11.003

Fowler, D., Pilegaard, K., Sutton, M.A., Ambus, P., Raivonen, M., Duyzer, J., Simpson, D., Fagerli, H., Fuzzi, S., Schjoerring, J.K., Granier, C., Neftel, A., Isaksen, I.S.A., Laj, P., Wichink-

kruit, R., Butterbach-bahl, K., Flechard, C., Tuovinen, J.P., Coyle, M., Gerosa, G., Palmer, P.I., Loreto, F., Ro-poulsen, H., Cellier, P., Cape, J.N., Horva, L., Rinne, J., Misztal, P., Nemitz, E., Nilsson, D., Pryor, S., Gallagher, M.W., Vesala, T., Zechmeister-boltenstern, S., Williams, J., Dowd, C.O., Skiba, U., Bru, N., 2009. Atmospheric composition change: ecosystems-atmosphere interactions. Atmos. Environ. 43, 5193–5267. https://doi.org/10.1016/j.atmosenv.2009.07.068

Friedlander, S.K., 1977. Smoke, Dust and Haze: Fundamentals of Aerosol Behavior. John Wiley & Sons Inc., New York.

Giardina, M., Buffa, P., 2018. A new approach for modeling dry deposition velocity of particles. Atmos. Enviroment 180, 11–22. https://doi.org/10.1016/j.atmosenv.2018.02.038

Hall, N.L., Dvonch, J.T., Marsik, F.J., Barres, J.A., Landis, M.S., 2017. An artificial turf-based surrogate surface collector for the direct measurement of atmospheric mercury dry deposition. Int. J. Environ. Res. Public Health 14. https://doi.org/10.3390/ijerph14020173

Hamilton, R.S., Mansfield, T.A., 1991. Airborne particulate elemental carbon: its sources, transport, and contribution to dark smoke and soiling. Atmos. Environ. 25, 715–723.

Hand, J.L., Schichtel, B.A., Malm, W.C., Pitchford, M.L., 2012. Particulate sulfate ion concentration and SO_2 emission trends in the United States from the early 1990s through 2010. Atmos. Chem. Phys. 12, 10353–10365. https://doi.org/10.5194/acp-12-10353-2012

Heard, A.M., Sickman, J.O., Rose, N.L., Bennett, D.M., Lucero, D.M., Melack, J.M., Curtis, J.H., 2014. 20th century atmospheric deposition and acidification trends in lakes of the Sierra Nevada, California, USA. Environ. Sci. Technol. 48, 10054-10061 https://doi.org/10.1021/es500934s

Holsen, T.M., Noll, K.E., 1992. Dry deposition of atmospheric particles: application of current models to ambient data. Environ. Sci. Technol. 26, 1807–1815. https://doi.org/10.1021/es00033a015

Holsen, T.M., Noll, K.E., Liu, S.P., Lee, W.-J., 1991. Dry deposition of polychlorinated biphenyls in urban areas. Environ. Sci. Technol. 25, 1075–1081. https://doi.org/10.1021/es00018a009

Horvath, H., Pesava, P., Toprak, S., 1996. Technique for measuring the depostion velocity of particulate matter to building surfaces 190, 255–258. https://doi.org/10.1016/0048-9697(96)05216-3

Huang, J., Lyman, S.N., Hartman, J.S., Gustin, M.S., 2014. A review of passive sampling systems for ambient air mercury measurements. Environ. Sci. Process. Impacts 16, 374–392. https://doi.org/10.1039/C3EM00501A

Im, U., Christodoulaki, S., Violaki, K., Zarmpas, P., Kocak, M., Daskalakis, N., 2013. Atmospheric deposition of nitrogen and sulfur over southern Europe with focus on the Mediterranean and the Black Sea. Atmos. Environ. 81, 660–670. https://doi.org/10.1016/j.atmosenv.2013.09.048

Kolesar, K.R., Mattson, C.N., Peterson, P.K., May, N.W., Prendergast, R.K., Pratt, K.A., 2018. Increases in wintertime $PM_{2.5}$ sodium and chloride linked to snowfall and road salt application. Atmos. Environ. 177, 195–202. https://doi.org/10.1016/j.atmosenv.2018.01.008

Kumar, P., Hopke, P.K., Raja, S., Casuccio, G., Lersch, T.L., West, R.R., 2012. Characterization and heterogeneity of coarse particles across an urban area. Atmos. Environ. 46, 449–459. https://doi.org/10.1016/j.atmosenv.2011.09.018

Lestari, P., Oskouie, A.K., Noll, K.E., 2003. Size distribution and dry deposition of particulate mass, sulfate and nitrate in an urban area. Atmos. Environ. 37, 2507–2516. https://doi.org/10.1016/S1352-2310(03)00151-1

Lewandowska, A., Falkowska, L., Jóźwik, J., 2013. Factors determining the fluctuation of fluoride concentrations in PM_{10} aerosols in the urbanized coastal area of the Baltic Sea (Gdynia, Poland). Environ. Sci. Pollut. Res. 20, 6109–6118. https://doi.org/10.1007/s11356-013-1592-2

Lindberg, S., Bullock, R., Ebinghaus, R., Engstrom, D., Feng, X., Fitzgerald, W., Pirrone, N., Prestbo, E., Seigneur, C., 2007. A synthesis of progress and uncertainties in attributing the sources of mercury in deposition. Ambio 36, 19–32.

Liteplo, R., Gomes, R., Howe, P., Malcolm, H., 2002. Fluorides (WHO Report). World Heal. Organ. 262. https://doi.org/10.1016/0043-1354(85)90052-1

Liu, C., Lin, S., Awasthi, A., Tsai, C., Wu, Y., Chen, C., 2014. Sampling and conditioning artifacts of $PM_{2.5}$ in filter-based samplers. Atmos. Environ. 85, 48–53. https://doi.org/10.1016/j.atmosenv.2013.11.075

Liu, C., Lin, S., Tsai, C., Wu, Y., Chen, C., 2015. Theoretical model for the evaporation loss of $PM_{2.5}$ during filter sampling. Atmos. Environ. 109, 79–86. https://doi.org/10.1016/j.atmosenv.2015.03.012

Liu, L., Zhang, X., Zhang, Y., Xu, W., Liu, X., Zhang, X., Feng, J., Chen, X., Zhang, Y., Lu, X., Wang, S., Zhang, W., Zhao, L., 2017. Dry particulate nitrate deposition in China. Environ. Sci. Technol. 51, 5572–5581. https://doi.org/10.1021/acs.est.7b00898

Livingston, R.A., 2016. Acid rain attack on outdoor sculpture in perspective. Atmos. Environ.

146, 332–345. https://doi.org/10.1016/j.atmosenv.2016.08.029

Lynam, M.M., Dvonch, J.T., Hall, N.L., Morishita, M., Barres, J.A., 2015. Trace elements and major ions in atmospheric wet and dry deposition across central Illinois, USA. Air Qual. Atmos. Heal. 8, 135–147. https://doi.org/10.1007/s11869-014-0274-7

MacLeod, M., Scheringer, C., Gotz, C., Hungerbuhler, K., Davidson, C.I., Holsen, T.M., 2011. Handbook of Chemical Mass Transport in the Environment, in: Thibodeaux, L.J., Mackay, D. (Eds.), Handbook of Estimation Methods: Environmental Mass Transport Coefficients. Taylor and Francis Group, New York, pp. 104–135.

Mamane, Y., Gottlieb, J., 1992. Nitrate formation on sea-salt and mineral particles—a single particle approach. Atmos. Environ. Part A 26A, 1763–1769. https://doi.org/10.1016/0960-1686(92)90073-T

McCready, D.I., 1986. Wind tunnel modeling of small particle deposition. Aerosol Sci. Technol. 5, 301–312. https://doi.org/10.1080/02786828608959095

Meira, G.R., Andrade, C., Padaratz, I.J., Alonso, C., Borba, J.C., 2007. Chloride penetration into concrete structures in the marine atmosphere zone- relationship between deposition of chlorides on the wet candle and chlorides accumulated into concrete. Cem. Concr. Compos. 29, 667–676. https://doi.org/10.1016/j.cemconcomp.2007.05.009

Mohan, M.S., 2016. An overview of particulate dry deposition: measuring methods, deposition velocity and controlling factors. Int. J. Environ. Sci. Technol. 13, 387–402. https://doi.org/10.1007/s13762-015-0898-7

Monteith, D.T., Stoddard, J.L., Evans, C.D., Wit, H.A. De, Forsius, M., Jeffries, D.S.,

Vuorenmaa, J., Keller, B., Wilander, A., Skjelkva, B.L., 2007. Dissolved organic carbon trends resulting from changes in atmospheric deposition chemistry. Nature 450, 10051–10064. https://doi.org/10.1038/nature06316

Nicholson, K.W., 1988. The dry deposition of small particles: a review of experimental measurements. Atmos. Environ. 22, 2653–2666.

Patra, A., Colvile, R., Arnold, S., Bowen, E., Shallcross, D., Martin, D., Price, C., Tate, J., ApSimon, H., Robins, A., 2008. On street observations of particulate matter movement and dispersion due to traffic on an urban road. Atmos. Environ. 42, 3911–3926. https://doi.org/10.1016/j.atmosenv.2006.10.070

Pitt, J.M., Schluter, M.C., Lee, D., Dubberke, W., 1987. Sulfate impurities from deicing salt and durability of portland cement mortar, in: 66th Annual Meeting of the Transportation Board. Transportation Research Board, Washington District of Columbia, pp. 16–23.

Raymond, H.A., Yi, S.M., Moumen, N., Han, Y., Holsen, T.M., 2004. Quantifying the dry deposition of reactive nitrogen and sulfur containing species in remote areas using a surrogate surface analysis approach. Atmos. Environ. 38, 2687–2697. https://doi.org/10.1016/j.atmosenv.2004.02.011

Roupsard, P., Amielh, M., Maro, D., Coppalle, A., Branger, H., Connan, O., Laguionie, P., Hebert, D., Talbaut, M., 2013. Measurement in a wind tunnel of dry deposition velocities of submicron aerosol with associated turbulence onto rough and smooth urban surfaces. J. Aerosol Sci. 55, 12–24. https://doi.org/10.1016/j.jaerosci.2012.07.006

Saliba, N.A., Chamseddine, A., 2012. Uptake of acid pollutants by mineral dust and their effect on aerosol solubility. Atmos. Environ. 46, 256–263.

https://doi.org/10.1016/j.atmosenv.2011.09.074

Saxena, A., Kulshreshta, U.C., Kumar, N., Kumari, K.M., Srivastava, S.S., 1992. Dry deposition of nitrate and sulphate on surrogate surfaces. Environ. Int. 18, 509–513. https://doi.org/10.1016/0160-4120(92)90269-A

Schlichting, H., Gersten, K., 2000. Boundary layer theory, 8th ed. Springer Berlin Heidelberg.

Schwede, D., Zhang, L., Vet, R., Lear, G., 2011. An intercomparison of the deposition models used in the CASTNET and CAPMoN networks. Atmos. Environ. 45. https://doi.org/10.1016/j.atmosenv.2010.11.050

Sehmel, G.A., 1973. Particle eddy diffusivities and deposition velocities for isothermal flow and smooth surfaces. J. Aerosol Sci. 4, 125–138. https://doi.org/10.1016/0021-8502(73)90064-5

Seinfeld, J.H., Pandis, S.N., 2016. Atmospheric Chemistry and Physics: From Air Pollution to Climate Change. John Wiley & Sons Inc., New York.

Settle, D.M., Patterson, C.C., 1982. Magnitudes and sources of precipitation and dry deposition fluxes of indestrial and natural leads to the North Pacific at Enewetak. J. Geophys. Res. Ocean. 87, 8857–8869. https://doi.org/10.1029/JC087iC11p08857

Sheu, H., Lee, W., Hwang, K.P., Liow, M., Wu, C., Hsieh, L., 1996. Dry deposition velocities of polycyclic aromatic hydrocarbons in the ambient air of traffic intersections. J. Environ. Sci. Heal. Part A Environ. Sci. Eng. Toxicol. 31, 2295–2311. https://doi.org/10.1080/10934529609376492

Slooff, W., Eerens, H.C., Janus, J.A., Ros, J.P.M., 1990. Integrated Criteria Document Fluorides.

Stelson, A.W., Seinfeld, J.H., 1982. Relative humidity and temperature dependence of the ammonium nitrate dissociation constant. Atmos. Environ. 16, 983–992.

https://doi.org/10.1016/0004-6981(82)90184-6

Tanner, P.A., Law, P.T., Tam, W.F., 2001. Comparison of aerosol and dry deposition sampled at two sites in Southern China. Atmos. Environ. 32, 4223–4233. https://doi.org/10.1016/S0021-8502(00)00091-4

Tasdemir, Y., Esen, F., 2007. Dry deposition fluxes and deposition velocities of PAHs at an urban site in Turkey. Atmos. Environ. 41, 1288–1301. https://doi.org/10.1016/j.atmosenv.2006.09.037

Tasdemir, Y., Günez, H., 2006. Ambient concentration, dry deposition flux and overall deposition velocities of particulate sulfate measured at two sites. Atmos. Res. 81, 250–264. https://doi.org/10.1016/j.atmosres.2006.01.002

Tasdemir, Y., Kural, C., 2005. Atmospheric dry deposition fluxes of trace elements measured in Bursa, Turkey. Environ. Pollut. 138, 463–473. https://doi.org/10.1016/j.envpol.2005.04.012

Tasdemir, Y., Odabasi, M., Vardar, N., Sofuoglu, A., Murphy, T.J., Holsen, T.M., 2004. Dry deposition fluxes and velocities of polychlorinated biphenyls (PCBs) associated with particles. Atmos. Environ. 38, 2447–2456.

Usher, C.R., Michel, A.E., Grassian, V.H., 2003. Reactions on Mineral Dust. Chem. Rev. 103, 4883–4939. https://doi.org/10.1021/cr020657y

Vitousek, P.M., Aber, J.D., Howarth, R.W., Likens, G.E., Matson, P.A., Schindler, D.W., Schlesinger, W.H., Tilman, D.G., 1997. Human alteration of the global nitrogen cycle: sources and consequences. Ecol. Appl. 7, 737–750. https://doi.org/10.1890/1051-0761(1997)007[0737:HAOTGN]2.0.CO;2

Wai, K.-M., Leung, K.-Y., Tanner, P.A., 2010. Observational and modeling study of dry deposition on surrogate surfaces in a South China city: implication of removal of atmospheric crustal particles. Environ. Monit. Assess. 164, 143–152. https://doi.org/10.1007/s10661-009-0881-1

Wolfe, M.F., Schwarzbach, S., Sulaiman, R.A., 1998. Effects of mercury on wildlife: a comprehensive review. Environ. Toxicol. Chem. 17, 146–160. https://doi.org/10.1002/etc.5620170203

Wolff, G.T., 1984. On the nature of nitrate in coarse continental aerosols. Atmos. Environ. 18, 977–981. https://doi.org/10.1016/0004-6981(84)90073-8

Wu, Y.-L., Davidson, C.I., Dolske, D.A., Sherwood, S.I., 1992a. Dry deposition of atmospheric contaminants: the relative importance of aerodynamic, boundary layer, and surface resistances. Aerosol Sci. Technol. 16, 65–81. https://doi.org/10.1080/02786829208959538

Wu, Y.-L., Davidson, C.I., Lindberg, S.E., Russell, A.G., 1992b. Resuspension of particulate chemical species at forested sites. Environ. Sci. Technol. 26, 2428–2435. https://doi.org/10.1021/es00036a014

Yang, H.H., Hsieh, L. Te, Cheng, S.K., 2005. Determination of atmospheric nitrate particulate size distribution and dry deposition velocity for three distinct areas. Chemosphere 60, 1447–1453. https://doi.org/10.1016/j.chemosphere.2005.01.067

Yang, H.H., Hsieh, L. Te, Lin, M.C., Mi, H.H., Chen, P.C., 2004. Dry deposition of sulfate-containing particulate at the highway intersection, coastal and suburban areas. Chemosphere 54, 369–378. https://doi.org/10.1016/S0045-6535(03)00655-6

Yao, X., Zhang, L., 2012. Chemical processes in sea-salt chloride depletion observed at a Canadian rural coastal site. Atmos. Environ. 46, 189–194. https://doi.org/10.1016/j.atmosenv.2011.09.081

Yi, S.M., Holsen, T.M., Noll, K.E., 1997. Comparison of dry deposition predicted from models and measured with a water surface sampler. Environ. Sci. Technol. 31, 272–278. https://doi.org/10.1021/es960410g

Yun, H., Yi, S., Kim, Y.P., 2002. Dry deposition fluxes of ambient particulate heavy metals in a small city, Korea. Atmos. Environ. 36, 5449–5458.

Zhang, L., Cheng, I., Wu, Z., Harner, T., Schuster, J., Charland, J., Muir, D., Parnis, J.M., 2015. Dry deposition of polycyclic aromatic compounds to various land covers in the Athabasca oil sands region. J. Adv. Model. Earth Syst. 7, 1339–1350. https://doi.org/10.1002/2015MS000473

Zhang, X., McMurry, P.H., 1992. Evaporative losses of fine particulate nitrates during sampling. Atmos. Environ. Part A, Gen. Top. 26, 3305–3312. https://doi.org/10.1016/0960-1685(92)90347-N

Zhuang, H., Chan, C.K., Fang, M., Wexler, A.S., 1999. Formation of nitrate and non-sea-salt sulfate on coarse particles. Atmos. Environ. 33, 4223–4233. https://doi.org/10.1016/S1352-2310(99)00186-7

Zufall, M.J., Davidson, C.I., Caffrey, P.F., Ondov, J.M., 1998. Airborne concentrations and dry deposition fluxes of particulate species to surrogate surfaces deployed in southern Lake Michigan. Environ. Sci. Technol. 32, 1623–1628. https://doi.org/10.1021/es9706458

Alexander J. Johnson

151 Link Hall, Syracuse University, Syracuse, NY 13244

ajjohn03@syr.edu ● (651)-470-2875 ● https://ajjohn03.expressions.syr.edu

EDUCATION

Syracuse University, Syracuse, New York, USA

M.S. Environmental Engineering (2018)

- Advisor: Dr. Cliff Davidson, Professor and Environmental Engineering Program Director
- Thesis: Measuring Atmospheric Dry Deposition to Urban Surfaces
- Cumulative GPA: 3.96/4.00

Iowa State University, Ames, Iowa, USA

B.S. Environmental Science (2014)

- Graduated with magna cum laude
- Cumulative GPA: 3.81/4.00

RESEARCH

Graduate Research Assistant, Syracuse University (2014-2018)

- Developed new method to measure dry deposition of dust
- Designed field and laboratory experiments to quantify pollutants in dust
- Supervisor: Dr. Cliff Davidson, Professor and Environmental Engineering Program Director

Undergraduate Research Assistant, Iowa State University (2013-2014)

- Focus: measured carbon fluxes to understand how natural vegetation minimizes erosion of soil
- Supervisor: Dr. Michael Castellano, Associate Professor

Research Assistant, Center for Sustainable Energy REU, University of Notre Dame (2012)

- Focus: synthesized radioactive crystals to understand their properties in the environment
- Supervisor: Dr. Peter C. Burns, Professor and Director of Center for Sustainable Energy

PUBLICATIONS

A. Johnson, and C. Davidson, *Chemistry of Stormwater Runoff from a Large Green Roof in Syracuse, NY*, in Proceedings of ASCE International Conference on Sustainable Infrastructure, Brooklyn, NY, pp. 45-52 Oct. 2017.

A. Johnson, *Evaluating the Effects of Perennial Grass Filter Strips (PFS) on Eroded Carbon Fluxes in Agricultural Watersheds*, in Iowa State University Undergraduate Research Symposium Repository, Ames, IA, 2014.

FELLOWSHIPS & AWARDS

Syracuse University EMPOWER NRT Fellowship (2016-2017)

Syracuse University Water Initiative Fellowship (2015-2016)

U.S. Dept. of Transportation TranLIVE University Consortium Student of the Year (2015)

PLATFORM PRESENTATIONS

A. Johnson, and C. Davidson, *Washoff of Dry Deposited Atmospheric Aerosol from a Traditional Roof and a Green Roof*, American Association for Aerosol Research 36th Annual Conference, Raleigh, NC, Oct. 19, 2017.

A. Johnson, and C. Davidson, *Deposition and Washoff of Atmospheric Trace Metals and Anions from Two Large Building Roofs*, American Association for Aerosol Research 35th Annual Conference, Portland, OR, Oct. 19, 2016.

A. Johnson and C. Davidson, *Influence of Urban Aerosols on the Chemistry of Stormwater Runoff*, American Association for Aerosol Research 34th Annual Conference, Minneapolis, MN, Oct. 13, 2015.

GRANTS

PI for Evaluating the Water and Energy Performance of the Center of Excellence (CoE) Green Roof, Syracuse University Office of Sustainability, Award: $14,000, Dates: 2017-2018

LEADERSHIP

Treasurer, ASEE Student Chapter, Syracuse University (2015-2018)

- Role: planned budget and skill development workshops for graduate students

Mentor, Center for Environmental Engineering Systems REU, Syracuse University (2014-

2018)

- Role: mentored undergraduate students and supervised their research projects

TEACHING

Teaching Assistant, Syracuse University (2014-2018)

- Courses: 1st Year Engineering Experience for Honors Students, Environmental Chemistry, Environmental Microbiology, and Sustainability in Civil & Environmental Systems
- Role: developed problems and class activities; facilitated recitations

PROFESSIONAL AFFILIATIONS

American Society of Engineering Education (ASEE): Student Member

American Association for Aerosol Research (AAAR): Student Member

Institute for Sustainable Infrastructure: Envision Sustainability Professional (ENV SP)

ANALYTICAL SKILLS

Computational: ANSYS Fluent, R

Laboratory Methods: Colorimetry, Ion Chromatography, Inductively-Coupled Plasma Mass Spectrometry, Electrochemical Measurements for pH